

# Substrate Roughness Significantly Affects Bilayer Phase Separation

*James A. Goodchild, Danielle L. Walsh, Simon D. Connell\**

School of Physics and Astronomy, University of Leeds, Leeds, United Kingdom

## **Abstract**

Supported Lipid Bilayers (SLBs) are model membranes formed at solid substrate surfaces. This architecture renders the membrane experimentally accessible to surface sensitive techniques used to study their properties, including Atomic Force Microscopy (AFM), Quartz Crystal Microbalance with Dissipation (QCM-D) and X-Ray/Neutron Reflectometry, and allows the bilayer to be integrated with technology for potential biotechnological applications, such as drug screening devices. From a biological function perspective, it could be argued that a supported bilayer is a more useful model of a biological cell membrane, which sits between the cytoskeleton and the extracellular matrix networks. Many substrates can be used to support lipid bilayers, dependent upon the experimental signal being measured. Simple lipid dynamics and structures on SLBs have been investigated, but there have been very few studies quantifying how different substrates can lead to different results. We present data showing that the phase separation of a well-studied lipid mixture varies drastically between mica and glass. The distinct micron scale domains observed on mica, very similar to those seen in free-floating Giant Unilamellar Vesicles

(GUVs), are reduced to nanometer scale domains on glass. The origin of this difference is not due to variations in molecular diffusion rate or to changes in thermal transition temperature, both of which would imply a chemical difference, but rather a hindering of the hydrodynamic flow of clusters or small domains during the process of phase separation. Nanoscale roughness with a radius of curvature too small for the bilayer to conform leads to pinning points where ordered domains are effectively arrested, and no longer able to coalesce via cluster/domain motion, limiting phase separation to molecular accretion. This hypothesis is confirmed by introducing defined roughness to a mica surface.

## Introduction

Model lipid membranes have been studied extensively to investigate the fundamental structure and physics of the cell membrane,<sup>1-3</sup> investigate protein and drug interactions with the membrane,<sup>4</sup> and to develop biotechnological applications such as drug delivery systems.<sup>5</sup> The ability to form Supported Lipid Bilayers (SLBs) on solid substrates renders them experimentally accessible to surface sensitive techniques, such as Atomic Force Microscopy (AFM),<sup>6</sup> Quartz Crystal Microbalance with Dissipation (QCM-D),<sup>7</sup> and Fluorescence techniques such as Fluorescence Correlation Spectroscopy (FCS)<sup>8,9</sup> and Fluorescence Recovery After Photobleaching (FRAP).<sup>10,11</sup> This has yielded information about lipid diffusion, lipid ordering, bilayer structure, and phase behaviour.<sup>6,9,12,13</sup> As the cell membrane is not isolated but sits between the cytoskeleton and the extracellular matrix networks,<sup>14,15</sup> controlled interaction with solid supports could give us the potential to tune bilayer properties to those of a biological cell membrane. Substrates can potentially be designed to replicate these rough, elastic and porous polymer networks.

Whilst it is recognised that substrates can affect bilayer properties compared to free-floating systems, the extent of the effect, the influence of experimental conditions, and even the interaction mechanism are not understood. Although there is a thin interstitial water layer between the bilayer and the substrate which allows the bilayer to remain fluid, the diffusion has been shown to drop for both mica and glass SLBs compared to free standing Giant Unilamellar Vesicles (GUV) and Black Lipid Membranes (BLM).<sup>2,16</sup> Phase separation can also change significantly in SLBs. This is important because the separation of immiscible lipid types into distinct phases with separate ordering, diffusion and lateral density has been linked with the potential existence of lipid rafts in the plasma membrane.<sup>17</sup> Lipid rafts are proposed to be responsible for biological processes such as signal transduction and protein clustering. Phase domains on solid supports can vary in shape and size compared to GUVs, and in particular domains appear to be static in SLBs due to an interaction with the surface.<sup>13,18</sup> Domains remain kinetically trapped in SLBs whereas domains in GUVs can collide and coalesce to form larger domains,<sup>13,18</sup> driven by the reduction in free energy due to the hydrophobic mismatch at the boundary between phases.

Strategies to decouple the bilayer from the substrate include double bilayers,<sup>10,19,20</sup> tethering of a free floating bilayer to a surface,<sup>21</sup> and supporting the bilayer on a hydrated polymer cushion.<sup>22</sup> Whilst these methods can be effective, they increase the complexity of the sample preparation, and are only suitable for certain techniques.

Many substrates can be used to support lipid bilayers including mica, glass and silicon, the choice usually driven by the signal being measured. AFM predominantly uses mica, a mineral that is easily cleaved to be atomically flat, enabling high z resolution of SLBs and their phases.<sup>23,24</sup> Fluorescence microscopy techniques are best utilised using glass, which is optically transparent.<sup>11,25</sup> Issues arise when comparing results between different surface sensitive techniques

due to the different substrates used. It is therefore imperative that the effect of substrate is understood and taken into account when interpreting and comparing the data arising from different experiments, between surface and free-floating bilayers, between different surface-sensitive instruments, and between research groups.

Phase behaviour has been well characterised on mica, to give information on domains such as size, height and dynamics.<sup>23,26,27</sup> However, reports of phase separation on glass are more scarce. Domains have been observed on glass from Langmuir-Blodgett Deposition,<sup>13,28,29</sup> where the domains are already present at the liquid-air interface before deposition, and in phase separated GUVs ruptured onto glass.<sup>13,25,30</sup> However, these domains do not re-form upon temperature cycling,<sup>13,25</sup> implying that interaction with glass kinetically traps a pre-existing phase structure at the moment of absorption, preventing further segregation. In the literature we have only found a few studies showing domains forming on glass via vesicle fusion, where the domains would have to nucleate and grow from a single homogenous phase on the substrate.<sup>8,11,31</sup> This is remarkable considering the ubiquitous use of glass in optical microscopy,<sup>12,32,33</sup> and the hundreds if not thousands of papers showing phase separation in free-floating GUVs,<sup>1,25,34</sup> and in SLBs on mica.<sup>18,23,24,26</sup>

In this study we find that DPPC/DOPC (60:40) bilayers form rough nanoscale domains on glass in contrast to micron scale fractal domains on mica. These nanoscale domains on glass are beyond the resolution of diffraction limited microscopy and are visualised by AFM. We find no difference in molecular diffusion on the different substrates but significant hindering of hydrodynamic lipid flow resulting in restricted domain growth. Increased roughness on glass is the likely cause of this restriction in hydrodynamic lipid flow, through local pinning points, curvature effects, and disruption of the interstitial water layer structure and dynamics. The transition temperature ( $T_m$ )

of DPPC is also slightly reduced on glass compared to mica, indicating a more disordered bilayer caused by the rougher substrate. In contrast to multiple studies, we do not observe decoupling of the  $T_m$  between the two bilayer leaflets due to the substrate.<sup>27,35</sup>

## Experimental Section

### Preparation of Lipid Vesicles

DOPC (1,2-dioleoyl-*sn*-glycero-3-phosphocholine), DPPC (1,2-dipalmitoyl-*sn*-glycero-3-phosphocholine) and 16:0 NBD PE (1,2-dipalmitoyl-*sn*-glycero-3-phosphoethanolamine-N-(7-nitro-2-1,3-benzoxadiazol-4-yl, ammonium salt) were purchased from Avanti Polar Lipids (Alabaster, AL). Texas Red DHPE (Texas Red 1,2-Dihexadecanoyl-*sn*-Glycero-3-Phosphoethanolamine, Triethylammonium Salt) was purchased from Thermo Fisher Scientific UK. DOPC, DPPC, Texas Red DHPE and 16:0 NBD PE were dissolved into individual 5mM  $\text{CHCl}_3$  stock solutions and then mixed together in the desired composition. The lipid mixture in  $\text{CHCl}_3$  was dried under nitrogen for 20 min and then kept under vacuum overnight. The dry film was then hydrated in ultrapure water (Milli-Q), vortexed for 30 min, heated in an oven at 50°C for 30min and then tip sonicated for 30 min at 4°C. The Small Unilamellar Vesicle (SUV) sample was then centrifuged at 3000rpm for 3 min, to remove SUVs from the metal sonicator tip sediment.

### Substrate Preparation

Round glass coverslips (Thermo Scientific, Menzel-Glaser) were prepared by bath sonicating in Decon detergent for 15 min, followed by 10 min piranha treatment (1:3  $\text{H}_2\text{O}_2$ : $\text{H}_2\text{SO}_4$ ), followed by 20min exposure to UV ozone (UVOCS Inc. UV Ozone Cleaning System). These coverslips were used as they were for the fluorescence flow cell and glued to a magnetic stub to be used on the AFM stage.

Mica (Agar Scientific) substrates were cleaved using scotch tape prior to use. The mica was cut to size to fit into the fluorescence fluid cell, and for AFM was glued to a magnetic stub. To etch mica, stubs were cleaved and placed in PTFE beakers with 40% Hydrofluoric Acid (HF) for 30 min. The beaker and mica stubs were then poured into a large amount of Sodium Bicarbonate (90g in 1L), and then thoroughly rinsed with de-ionised water. This method was developed as a calibration tool for AFM.<sup>36</sup> A colleague trained in the safe handling of HF performed this procedure for us.

## **Supported Bilayer Formation**

For fluorescence measurements, glass or mica substrates were assembled into a home-built flow cell consisting of a sealed incubation chamber around the substrate and an inlet and outlet for flowing the sample in and washing. 1mL of 1mg/mL lipid vesicles were syringed into the cell. The vesicles were incubated on the surface for 30min (room temperature for DOPC, 50 °C for DPPC/DOPC). 1mL 20mM MgCl<sub>2</sub> at the same temperature was added for a further 30min. The sample was then allowed to cool to room temperature before the surface was washed to remove any unfused vesicles. A pump was connected to flow room temperature MiliQ water through at approx. 1mL/min for 30min.

For AFM measurements, 100 µL of SUV solution was deposited onto a freshly cleaved mica disk and incubated in a sealed humidity chamber for 1h at 50°C. Halfway through incubation 100 µL 20mM MgCl<sub>2</sub> was added. After incubation, the bilayer was cooled to room temperature and rinsed to remove any unruptured vesicles. MiliQ water, at the same temperature as the incubated bilayer, was washed across the surface 10 times in 50 µL bursts of a pipette.

The temperature of the bilayers was measured using a K-type thermocouple positioned to be in the buffer, close to the substrate in both the fluorescence fluid cell and the AFM incubation dish.

The Cooling rates were determined by taking the gradient between 33-29 °C , this is the transition temperature range of DPPC/DOPC (60:40), determined using published DPPC/DOPC temperature Phase Diagrams.<sup>1,37</sup> 0.25 deg/min was the cooling rate achieved by taking the fluid cell or incubation dish out of the oven at 50°C and allowing the bilayers to cool ambiently in the lab where the temperature was 21°C. 0.08°C was the cooling rate achieved by turning off the oven and letting both the oven and bilayers cool down to room temperature. The cooling rate for pure DPPC samples was calculated between 45-35 °C to match the  $T_m$  of pure DPPC, and is faster than the cooling rate between 33-29 °C to match the  $T_m$  of DPPC/DOPC (60:40). Standard Errors for cooling rates =  $0.080 \pm 0.008$  °C/Min (N=4),  $0.25 \pm 0.02$  °C/min (N=3).

## **Fluorescence and FRAP (Fluorescence Recovery after Photobleaching)**

Fluorescence Microscopy was performed using a Nikon Eclipse E600 microscope with an Andor Technology Zyla cCMOS camera. The microscope was equipped with a Mercury Lamp and filter cubes suitable for Texas Red (Ex. 540-580, Em. 600-660) and NBD (Ex. 465-495, Em. 515-555).

For Fluorescence Recovery after Photobleaching (FRAP) measurements, an aperture was used to bleach a 30um diameter spot with white light for 30sec. After photobleaching images were taken at 3sec intervals for 3min. Analysis was performed using a custom macro written for ImageJ, which compares the fluorescence intensity recovery to a reference area of non-bleached bilayer. The exponential recovery is fitted to obtain a recovery half life ( $t_{1/2}$ ), which can then be converted to a diffusion coefficient (D).

$$D = \gamma_D \left( \frac{r^2}{4t_{1/2}} \right)$$

Where  $r$  is the radius of the bleach spot and  $\gamma_D$  is a constant (0.88) related to the circular bleach shape.

The diffusion coefficient values presented are averages of several repeat runs (Glass N=12, Mica N=6), where for each repeat run the value is an average of at least 5 different areas from the substrate.

For Transition Temp Determination, DPPC bilayers were formed in the flow cell, as described earlier. After the wash at room temperature, the bilayer was heated up to 60°C and then FRAP videos obtained as it cooled. Diffusion Coefficient vs. Temperature plots were fitted to a Boltzmann Sigmoidal curve.

$$D = A_2 + \frac{A_1 - A_2}{1 + e^{\frac{T-T_0}{dT}}}$$

Where  $A_1$  and  $A_2$  are the y values of the flat fit above and below sigmoid curve and  $T_0$  is the turning point/midpoint of the curve, which is taken as value of  $T_m$ .

## Atomic Force Microscopy (AFM)

AFM Images were acquired using a Bruker Dimension with an ICON head. Bruker ScanAsyst Fluid probes (0.7 N/m, 150 kHz) were used. Imaging was performed using Peak Force Tapping mode in liquid using the ICON fluid tip holder. The AFM and Fluorescence images of the same bilayer sample area in Figure S3 were acquired using a Bruker Resolve AFM integrated with an inverted confocal microscope.

## Image Analysis

Fluorescence Microscopy images were analysed and processed using the FIJI distribution of ImageJ (NIH). AFM images were analysed using Nanoscope Analysis V1.9. AFM images were flattened using the appropriate order of levelling for each image. Power Spectral Density Spectra



of AFM substrate images were measured using a built in Nanoscope function. This function plots the power of height fluctuations against frequency, giving a quantitative measure of roughness at different length scales (Figure 6C).  $R_a$  roughness was measured using a built in Nanoscope function. The size of the image can affect the roughness calculation, so averages were taken from several images all at the same 5 $\mu$ m length scale for both substrates. Domains sizes were estimated by fitting an ellipse to the domain using ImageJ or Nanoscope Analysis, and then taking the average of the long and short radii of the ellipse (Figure S1)

The Radially Averaged Correlation Function was calculated from AFM images flattened in Nanoscope and then exported to ImageJ. The images were converted to a binary image of two phases using the threshold tool on ImageJ. The Binary image was run through a Radially Averaged Autocorrelation Function Macro (Michael Schmid, 27/9/2011 update) to produce an autocorrelation plot, giving a radially averaged quantitative measure of the length scale between black and white pixels i.e. the two different phases. This plot was fitted to an exponential decay using Origin Pro 9.1 to give a characteristic correlation length.

$$f(r) = Ae^{\frac{-r}{\xi}}$$

Where  $f(r)$  is the autocorrelation,  $r$  is distance and  $\xi$  is correlation length. Figure S2 shows the process of calculating correlation length from an AFM image.

This correlation length method was used for domains on glass, which due to their complex morphologies could not be fit individually to calculate domain size. The correlation length for the larger fractal gel domains on mica underestimates the domain size compared to domain size fitting. This is due to the domain protrusions resulting in a shape where each dark domain pixel is closer to a white non-domain pixel, thus a smaller correlation length. Comparing the correlation length to domain fitting, if you start at the centre of a domain (average of all positions), the nearest

opposite colour pixel is roughly half a radius away from the centre. Although the absolute number of the correlation length underestimates domain size, approx. 1.3 times for fluorescence images and approx. 2.4 times for AFM images, it provides a quantitative measure of length scale which scales with the increase in domain size. The correlation lengths of domains on mica measured by fluorescence and AFM are similar but not identical, explained due to the lower resolution of fluorescence compared to AFM. The domain protrusions are not always adequately resolved optically, and the correlation length measurement is more representative of a sphere of filled in shape, which has a longer distance from dark domain pixels to light non-domain pixels. There will also be a slight experimental variation in cooling rate between different runs. The size and density of domains on glass was not homogenous, shown later in Figure 2B and 3A. Larger scans like these enabled the heterogeneity to be seen over the micron scale, however the pixel density in these images was too low to allow accurate thresholding for correlation length analysis. Therefore, a statistical spread of smaller size images with larger pixel density were analysed.

## **Contact Angle**

Static Contact Angle measurements were taken using a First Ten Angstroms FTA 4000 CAG. An approx. 0.2 $\mu$ L droplet of MiliQ water was pipetted onto the surface and an image captured. The contact angle of the water with the mica and glass substrates was measured using fitting algorithms in the FTA 400 CAG software, to give the contact angle made between the surface and droplet. For mica N=18 (three repeats on six mica stubs) and for glass N=9 (three repeats on three glass cover slips).

## **DSC**

DPPC was dissolved in CHCl<sub>3</sub>, aliquoted into set amounts, dried under nitrogen and then left under vacuum overnight. The dry DPPC was hydrated with MiliQ water to 1 mg mL<sup>-1</sup> and vortexed

for 5 min to form large multilamellar vesicles (LMVs). The vesicle solution was degassed using a ThermoVac degasser (2x5min). Thermograms were obtained using a MicroCal VP-DSC. Continuous temperature cycles from 10-60 °C and then 60-10 °C were performed at 90 °C/hr, with a 15min equilibration period at 10 °C and 60 °C before each new scan. The filtering period was set to 10 s and feedback mode to high. To ensure the thermal history of both the reference and sample cells was similar, both cells were temperature cycled overnight with water prior to first measurement. For analysis, the baseline of the data was flattened using a mathematical fit on origin.

## Results and Discussion

### Phase Separation is Different on Mica and Glass

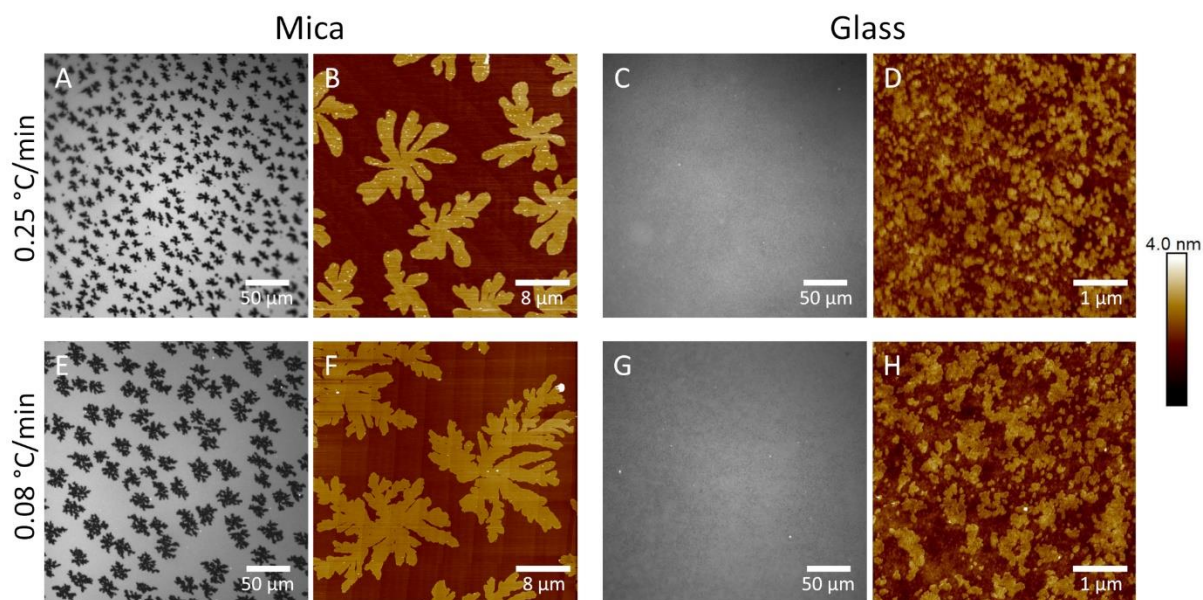


**Figure 1.** DPPC/DOPC (60:40) SLBs imaged with AFM (B,D,F,H) and DPPC/DOPC (60:40) + 0.5%TR SLBs imaged with fluorescence (A,C,E,G). A, B,E,F are on mica and C,D,G,H are on glass. The AFM images on glass are representative examples from a heterogeneous surface, with further examples given in Figure S5. The XY scales are indicated on all images with a

**scale bar. The Z range of all the AFM images is 4 nm, for reference the step height of domains in image B = 1.1 nm. The cooling rates from incubation temperature to room temperature are shown on the left-hand side and apply to the whole row. A-H are 8 separate experiments i.e. A and B are not the same sample, but the same lipid mixture incubated similarly for two different techniques.**

DPPC/DOPC (60:40) supported lipid bilayers were prepared on both freshly cleaved mica, and on a Piranha and UV Ozone cleaned glass substrate. The Fluorescence Microscopy images on mica show clear gel-liquid phase separation, with the fractal domain morphology matching closely to DPPC/DOPC domains in the literature.<sup>26</sup> The TR-DHPE dye associates preferentially with the fluid phase lipids (bright areas) and is excluded from the tightly packed gel domains (dark areas) (Figure 1A). AFM images, which can image the 1.0-1.5 nm variation in bilayer height between the tightly packed, taller gel phases and the shorter fluid phase, show the same gel phase domain morphology (Figure 1B). The two sets of domains, formed separately for different techniques but with the same incubation conditions, have a similar average radius (Table 1). Figure S3 shows AFM and Fluorescence images of the same bilayer area, proving that the domains observed by the two techniques are the same. When the same DPPC/DOPC (60:40) lipid mixture was identically incubated on a glass substrate, fluorescence images showed no clear phase separation (Figure 1C). FRAP confirmed that freely diffusing bilayers had formed. Imaging with AFM enabled a much higher resolution and confirmed that domains had formed on the glass substrate but were below the diffraction limit of the fluorescence microscope. The domains formed on glass (Figure 1D) have a significantly smaller length scale and show rough domain boundaries, compared to the larger domains with smooth boundaries and fractal morphologies on mica.

| Substrate | Cooling Rate (°C/min) | Domain Radius (AFM)                 | Domain Radius (Fluorescence) | Correlation Length (AFM) | Correlation Length (Fluorescence) |
|-----------|-----------------------|-------------------------------------|------------------------------|--------------------------|-----------------------------------|
| Mica      | 0.25±0.02             | 5.3±0.2 $\mu\text{m}$               | 4.57±0.04 $\mu\text{m}$      | 2.26±0.4 $\mu\text{m}$   | 3.2±0.2 $\mu\text{m}$             |
| Mica      | 0.080±0.008           | 8±1 $\mu\text{m}$                   | 8.9±0.2 $\mu\text{m}$        | 3.31±0.09 $\mu\text{m}$  | 7.3±0.1 $\mu\text{m}$             |
| Glass     | 0.25±0.02             | Domains connected so analysis fails | Resolution too low           | 74±5 nm                  | Resolution too low                |
| Glass     | 0.080±0.008           | Domains connected so analysis fails | Resolution too low           | 65±7 nm                  | Resolution too low                |

**Table 1. Domain Sizes and Correlation Lengths for Mica and Glass bilayers at different cooling rates.**

#### **Domain fitting and correlation length methods can be found in Experimental Section**

It should be highlighted how extreme the contrast in length scales between the domains formed on glass and mica are. This is shown both by AFM images with the same X,Y and Z scales in Figure 2, but also using correlation length analysis. The partially interconnected morphology of the domains on glass meant that fitting the domains to ellipses, as was done for the micron size domains on mica, was impossible. Correlation length analysis has been used previously to measure the length scales of critically fluctuating bilayer mixtures.<sup>23,38</sup> When a two phase bilayer image is converted to a binary black and white image, the correlation length is a radially averaged quantitative measure of the length scale between black and white pixels i.e. the two different phases. The average AFM image correlation length of domains on glass was 74±5 nm, but almost 2 orders of magnitude larger for domains on mica at 2.26±0.4  $\mu\text{m}$  (Table 1).

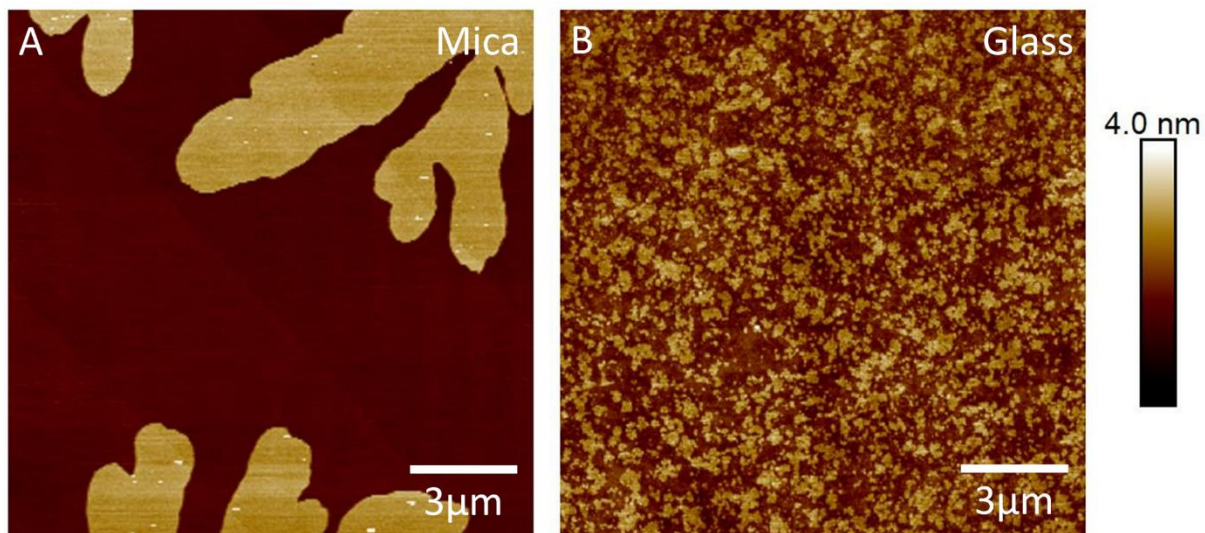


**Figure 2. DPPC/DOPC (60:40) SLBs on mica (A) and glass (B), highlighting the discrepancy in size and morphology of domains. X,Y and Z scales of the two images are the same. Z scale is 4nm. Both A and B were cooled at  $0.25 \pm 0.02$  °C/min.**

Visualising the nanoscale domains on glass optically is challenging due to the diffraction limited optics. When zoomed in, the fluorescence images of bilayers on glass show a fine speckled structure (Figure 3C). Even though the correlation length of the domains is only  $74 \pm 5$  nm, there is a heterogeneity in domain sizes and also aggregation of domains. This results in features that are just on the resolution threshold. An AFM image (Figure 3A) of the same size as the optical image was converted to greyscale and contrast adjusted such that the gel domains have a dark grey/black intensity identical to the large domains depleted of dye in the fluorescence images, and the background fluid phase appears light grey in a similar manner. The AFM image was then blurred using a 500 nm Gaussian filter, approximating the diffraction limiting effects of the wavelength of light used to image. The result of this AFM image processing is shown in Figure 3B, and as can be seen the observable pattern made by domains is similar to the optical image (bearing in mind they are not the exact same area and the domains on the surface are inhomogeneous). This shows

that although the fluorescence images show a speckled pattern rather than domains, these speckles are the result of nanoscale domains below optical resolution.

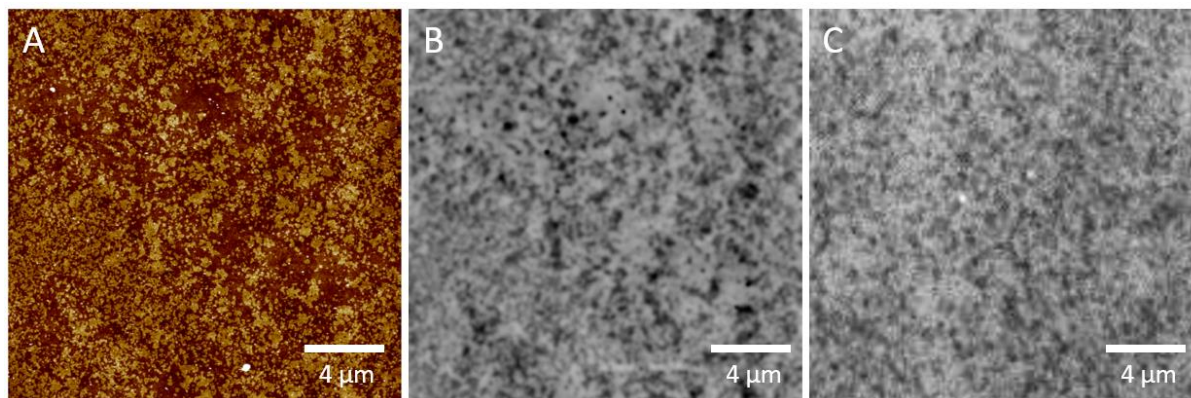


**Figure 3. A) AFM image of DPPC/DOPC (60:40) bilayer on glass. Cool rate is 0.08°C/min. Z scale is 4nm B) The AFM image A changed to greyscale and put through a 500nm gaussian blur, mimicking the diffraction limit of a microscope. C) Fluorescence microscope image of DPPC/DOPC (60:40) on glass, zoomed in to same size as AFM image A. Cool rate is 0.08±0.008°C/min. Scale bars are shown on all images.**

### **Single Lipid Gel Phase Structure is also different on Mica and Glass**

To investigate how molecular diffusion might affect domain formation we first studied simple single component lipid bilayers. Interestingly, during these experiments we noticed that in pure DPPC +16:0 NBD PC bilayers cooled from the melt, the dye was preferentially segregated during domain growth. This left behind a signature of domains with the same shape as the DPPC domains in the mixed DPPC/DOPC system (Figure 4). We attribute the structure to exclusion of the sterically bulky head-group fluorophore from the crystallising solid phase. Pure DPPC bilayers with a different dye, TR-DHPE, show similar behaviour. The much bulkier Texas Red group however is excluded from the crystallising DPPC even more vigorously, leading to a much more concentrated and thinner boundary around the nucleated domains and not a gradient. The final

remnant of liquid phase to freeze contains all of the TR-DHPE. Above the  $T_m$ , DPPC is in the fluid phase and mixes with the dye molecules, shown by a homogenous phase. As the bilayer cools through DPPC's  $T_m$  (40-41°C), pure DPPC crystallises excluding the DPPC molecules containing the fluorophore (Figure S4). Sufficiently below the  $T_m$  and at room temperature all the molecules are crystallised, as the dyes have the same PC chains. With NBD dye, this leaves the original nucleated domains of pure DPPC surrounded by an increasing gradient of dye, with the final remnants to freeze containing the highest concentration of dye. With TR, the dye is almost completely excluded from the nucleated DPPC domains.

When DPPC +16:0 NBD PC and DPPC +TR-DHPE were formed on glass, no structure was observed optically. Even the fluid phase TR-DHPE dye that was significantly excluded from pure DPPC on mica, does not show any separation on glass optically. As with the phase separated systems, the glass substrate is hindering the growth of lipid structures compared to mica. There have not been many studies showing a pure lipid bilayer excluding a lipid dye, perhaps due to the ubiquitous use of glass, where the exclusion might not be noticed due to the sub diffraction limit structures. However similar gel-like structures of cationic lipids excluding dyes were observed by McKienan et al.<sup>39</sup> and Crane et al. note the exclusion of dyes from the gel phase during compression in a Langmuir Trough.<sup>29,40</sup>



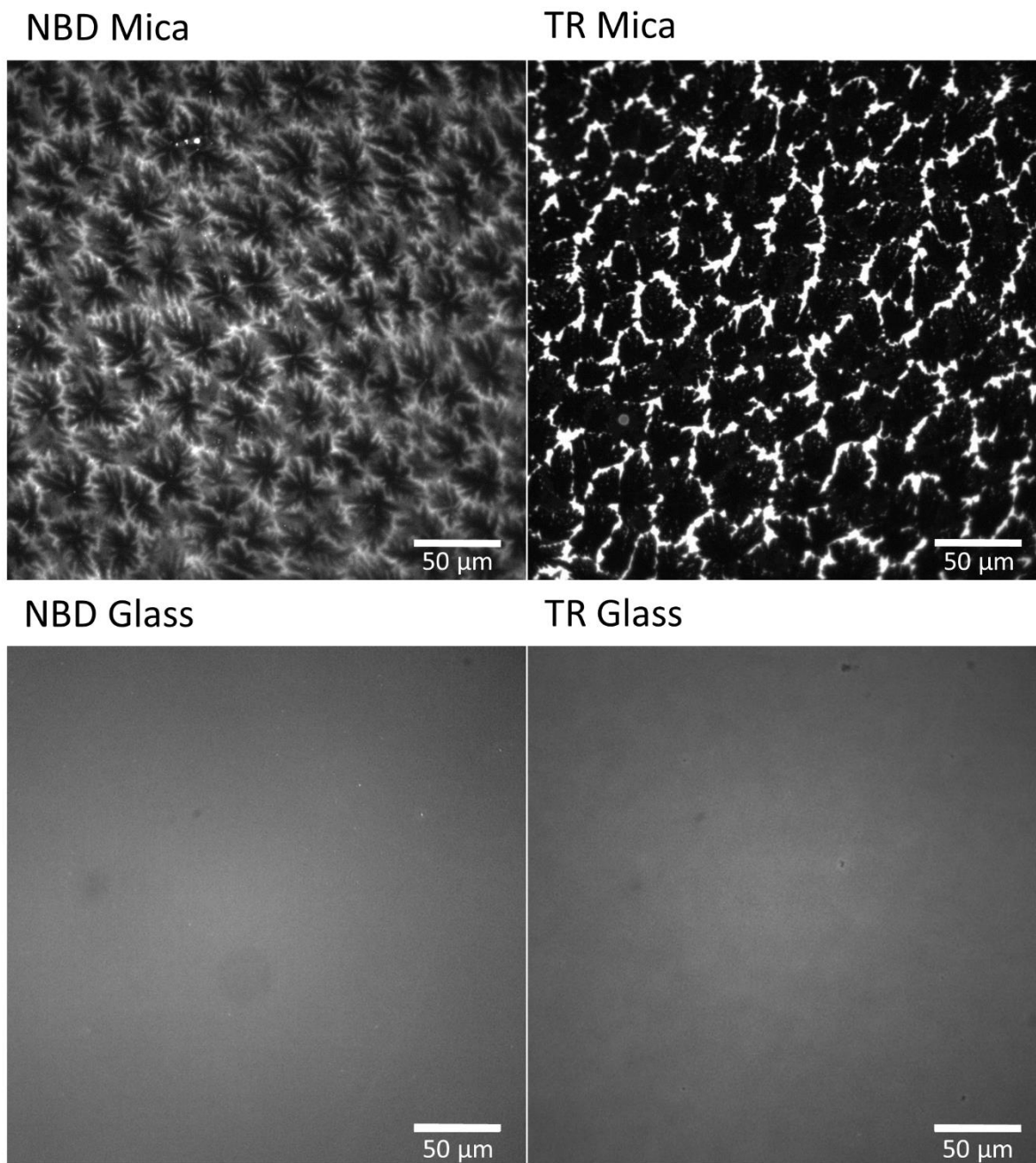


**Figure 4. Room Temperature Images of DPPC with 0.5mol% NBD or 0.5mol% TR. On mica DPPC domains are observed, as they have nucleated the dye molecules have been excluded. The bulky TR dye is more excluded than the smaller NBD dye. On glass no exclusion is observed, likely because it is below the diffraction limit.**

## Difference in Phase Separation between Mica and Glass is not due to Molecular Diffusion Rate

To understand the factors affecting domain sizes on the different substrates, we investigated single molecule dynamics on glass and mica. Fluorescence Recovery after Photobleaching (FRAP) was performed on DOPC + 0.5mol% TR-DHPE bilayers. The diffusion coefficients on mica ( $0.96 \pm 0.04 \mu\text{m}^2/\text{s}$ ) and glass ( $1.02 \pm 0.04 \mu\text{m}^2/\text{s}$ ) were remarkably similar. The diffusion coefficients of DPPC + 0.5mol% 16:0 NBD PE above its  $T_m$  on mica ( $2.1 \pm 0.1 \mu\text{m}^2/\text{s}$ ) and glass ( $2.1 \pm 0.3 \mu\text{m}^2/\text{s}$ ) were also the same. Our diffusion values match with literature values from different techniques, which vary between  $0.5\text{--}5.0 \mu\text{m}^2/\text{s}$  for fluid lipid systems.<sup>2,9,33,41</sup> FCS experiments have also found that DOPC diffusion is the same on glass and mica, all other experimental parameters being identical.<sup>9</sup> Harb et al. find DPPC FRAP diffusion on glass and mica to be the same when high ionic strength buffers are used, but it is faster on glass when ionic strength is low.<sup>42</sup> These two studies vary in bilayer deposition technique, the first using Vesicle Fusion (same as this paper), the second using Langmuir Blodgett Deposition, and this can potentially affect bilayer properties. Also, the different ionic strengths of buffers used clearly affect bilayer-substrate interactions. For our system where we use the same lipid, dye, buffer, deposition technique, equipment and analysis methods, we can say that molecular diffusion is not affected by the different substrates, so cannot be affecting the growth of different size domains.

As the FRAP data shows that overall lipid diffusion is not hindered on glass, we attempted to produce larger domains by using slower cooling rates, giving more time for the growth phase following nucleation. Decreasing the cooling rate through the miscibility transition temperature ( $T_m$ ) has been shown to increase the size of domains formed on mica.<sup>24,43</sup> Moving through  $T_m$  more slowly, allows more time for lipids to diffuse towards and attach to an expanding nucleating domain, creating larger domains with larger area to perimeter ratios and thus lowering the free

energy due to hydrophobic mismatch between phases. A faster quench through the  $T_m$  however, means there is less time for lipids to diffuse and they are kinetically trapped into many smaller nucleated domains. As expected, when the cooling rate from incubation temperature ( $50^\circ\text{C}$ ) down to room temperature was slowed from  $0.25\pm 0.02^\circ\text{C}/\text{min}$  to  $0.080\pm 0.008^\circ\text{C}/\text{Min}$ , the size of the gel domains on mica increased both in AFM and Fluorescence experiments (Figure 1 A to E and B to F and Table 1). The correlation length of domains on mica was shown to increase by 46% as cooling rate was slowed, matching closely to the increase of 51% in domain size fitting, confirming that correlation length is a good quantitative indicator of length scale. Importantly, the average correlation length on glass does not increase as the cooling rate is increased (Figure 1 and Table 1). The images in Figure 1 are example images, Figure S5 highlights the heterogeneity of different substrate areas. The correlation length averaged across repeat images produces similar values for both cooling rates. Even though there is more time for molecular lipid diffusion, larger domains do not form. The glass substrate is the limiting factor hindering the formation of larger domains.

## **Molecular Ordering is affected by Different Substrates**

Next, we investigated if the substrates were influencing the molecular ordering of the lipids. An experiment was designed to determine the transition temperature ( $T_m$ ) of a DPPC bilayer on both glass and mica using FRAP (similar to methods used before<sup>10,44</sup>), as  $T_m$  gives a quantitative measure of molecular ordering in a bilayer. DPPC was chosen instead of DPPC/DOPC (60:40) due to the sharper co-operative melting transition of pure lipids. The  $T_m$  value is about  $20^\circ\text{C}$  above room temperature, making it easy to observe. The  $T_m$  of free-floating DPPC Multilamellar Vesicles (MLVs) was characterised first using Differential Scanning Calorimetry (Figure 5A). DPPC shows a sharp melting point at  $41.72\pm 0.05^\circ\text{C}$  and sharp freezing point at  $39.73\pm 0.02^\circ\text{C}$ , with a  $1.5^\circ\text{C}/\text{min}$  ramp rate. These values match DPPC values from literature for MLVs and Large Unilamellar

Vesicles (LUVs), where the same dependence of heating and cooling rates on  $T_m$  offset is also observed.<sup>3,45,46</sup> DSC instruments have a finite capacity to transfer heat from heat source to the sample or vice versa, and if the heat required for a thermotropic transition exceeds this, the measured temperature will lag behind.<sup>47</sup> On the heating scan the  $T_m$  is offset to a higher temperature and on the cooling scan the  $T_m$  is offset to a lower temperature. It is widely known that slower cooling rates would reduce these offsets.

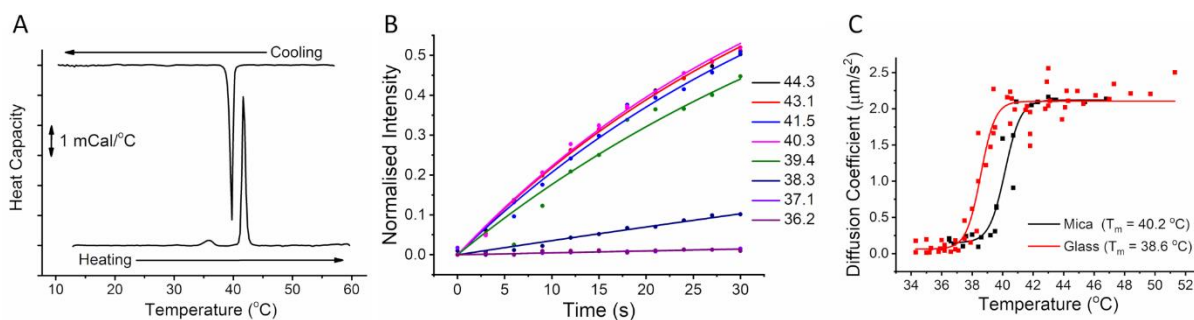


**Figure 5. Transition Temperature Determination. A) Differential Scanning Calorimetry (DSC) of DPPC MLVs showing the change in Differential Power/Heat Capacity with heating and Cooling. The peaks correspond to the gel-liquid transition temperature of the lipid (Heating cycle shows a pre-transition due to an interdigitated ripple-phase) with a sharp main transition peak at 41.65 (this image) and  $41.72 \pm 0.05$  (Average,  $N=5$ ). The cooling cycle shows a transition at 39.75 (this image) and  $39.73 \pm 0.02$  (Average,  $N=3$ ) B) An example run of FRAP Fluorescence Recovery over time curves for DPPC+ 0.5mol% NBD SLB on glass as the bilayer cools, with exponential recovery fit C) Calculated Diffusion coefficients (D) at each temperature for mica and glass, plotted against temperature. For Mica 4 repeat runs are plotted, for glass 5 repeat runs. Data fitted to a Boltzmann sigmoid,  $T_m$  value taken as midpoint of sigmoid.  $T_m$  values are averages of all repeats**

A DPPC SLB was formed on mica and cooled from 50 °C down to room temperature through  $T_m$ , performing FRAP at regular intervals (Figure S8). Above  $T_m$  the bleached FRAP area recovered as it was in a fluid phase and could freely diffuse. Below  $T_m$  the bleached spot did not recover or recovered very slowly, indicative of a gel phase. Fitting the exponential recoveries allowed Diffusion Coefficients to be calculated, which could then be plotted against temperature (Figure 5). A sigmoidal fit of this data revealed where the transition occurred (taken as the midpoint of the curve). The transition temperature determined by this method for mica was  $40.2 \pm 0.3$  °C (N=4). This value is close to the cooling scan DSC value for MLVs,  $39.73 \pm 0.02$  °C. The cooling rate for the FRAP Fluid Cell (0.6 °C/min) was slower than the DSC (1.5 °C/min) and the measured  $T_m$  from the FRAP is less offset towards lower temperatures, so this small difference is likely accounted for by the different cooling rate. This finding that the  $T_m$  of a lipid bilayer on mica is virtually identical to in free floating GUVs or MLVs is broadly replicated in other FRAP-with-temperature studies.<sup>10,42,44</sup>

The  $T_m$  determined by FRAP on glass was  $38.6 \pm 0.2$  (N=5). There is a small but significant drop in  $T_m$  of 1.6 °C from mica,  $40.2 \pm 0.3$  °C (N=4), to glass. This implies a disordering of the lipid molecules within the bilayer on glass compared to mica. The second bilayer in DPPC double supported bilayers has been shown to have a 1.4°C higher  $T_m$  than single bilayer SLBs on glass, more evidence that  $T_m$  is reduced slightly by proximity to the glass surface.<sup>10</sup> A reduction of 2°C in the  $T_m$  of DPPC supported on glass-like Silica beads compared to MLVs has also been observed.<sup>46</sup> In contrast, recent results have shown an increase in the  $L_o$ - $L_d$  miscibility  $T_m$  when a GUV is ruptured onto a glass surface, implying an increase in order.<sup>25</sup> Further study is needed to link substrate effects with both single lipid  $T_m$  and  $T_m$  in phase separated mixtures, as well as examining the effects of bilayer deposition methods on these values.

What is the origin of this disordering effect? One possibility is that the chemical nature of the surfaces may be influencing domain formation and bilayer order. The contact angle is a measure of the hydrophilicity of the surface and the density of hydrophilic functional groups i.e. hydroxyl groups. Hydrophilic surfaces have contact angles close to  $0^\circ$ , hydrophobic surfaces around  $90-110^\circ$ . The contact angles of the substrates were measured, with mica =  $3.0 \pm 0.2^\circ$  after cleavage, and glass =  $4.8 \pm 0.4^\circ$  after Piranha and UV ozone cleaning. There is little difference, both surfaces are hydrophilic before the vesicles are deposited and the bilayer is formed. This is unlikely to be having any effect on ordering or dynamics. We also show using contact angle how successive cleaning treatments are needed to form the most hydrophilic glass possible for bilayer formation. (Table 2). A contact angle of  $< 30^\circ$  is required for formation of a lipid bilayer via vesicle fusion.

| Washing Steps         | No wash    | Water Rinse | Decon Rinse | Decon +Piranha | Decon +Piranha +UV Ozone |
|-----------------------|------------|-------------|-------------|----------------|--------------------------|
| Average Contact Angle | $83 \pm 2$ | $56 \pm 2$  | $36 \pm 1$  | $17 \pm 2$     | $4.8 \pm 0.4$            |

**Table 2. Contact Angle Measurements of glass cover slips after successive cleaning steps.**

**N=9 for all (3 repeats on 3 different glass cover slips).**

### **Substrate Roughness is linked to Domain Size**

We used AFM images to measure the roughness of mica and glass, to see if roughness could be affecting domain formation and bilayer ordering. The  $R_a$  roughness of glass ( $0.148 \pm 0.004$  nm) after piranha cleaning and UV ozone cleaning is over 4 times rougher than the mica ( $0.029 \pm 0.002$  nm) after cleavage (Figure 6 A+B). These values match closely to previous AFM roughness

measurements of mica,<sup>12,41</sup> and piranha cleaned glass.<sup>11</sup> Power density spectra, which quantify roughness versus wavelength, are shown for the 3D surface topography AFM images of glass and mica (Figure 6C), showing that the roughness is larger on glass than mica across all length scales. Glass samples from different manufacturers can vary significantly in terms of surface structure (Figure S7), one of the reasons why a harsh chemical etch is so necessary. The glass used in this study as well as the glass used in literature reports, also shows nanoscale hole defects (Figure S6 and S7), observed but not thoroughly discussed in other literature reports.<sup>12,48,49</sup>

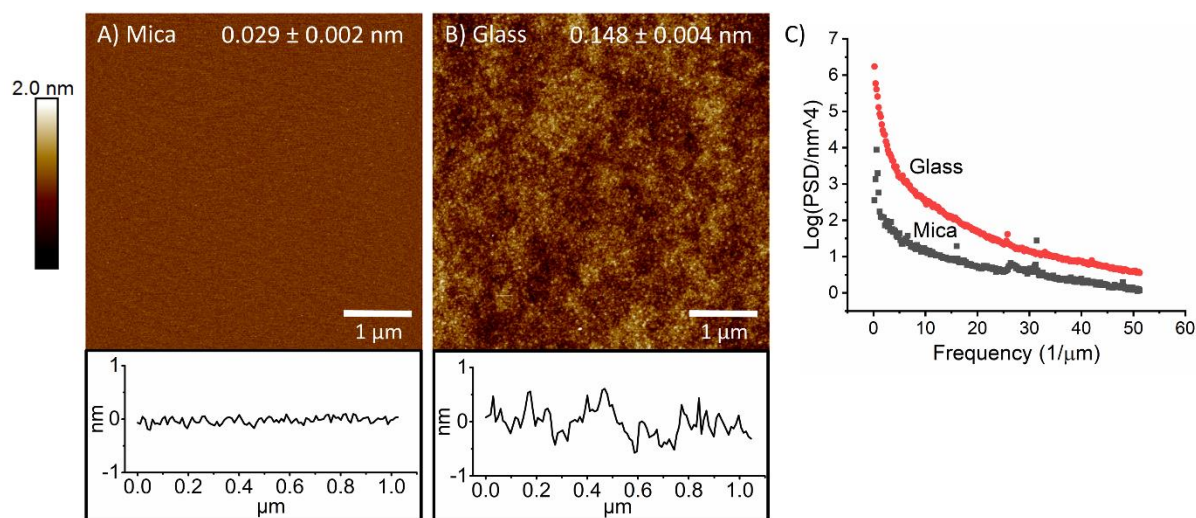


**Figure 6. AFM images of mica after cleavage (A) and Glass after Pirnaha and UV ozone clean (B). The Ra roughness measurements averaged over repeat images are included in top right of images. Individual AFM line scans are icluded below images. Scale bars are included on images, Z scale for A and B is 2 nm. C is A power Spectral Denisty Plot with Frequency, highlighting that the roughness is higher for glass over mica for all length scales.**

To confirm whether the difference in domain formation on rougher glass as compared with smooth mica was actually due to the roughness, and not some chemical difference, a method was devised to introduce a controlled degree of roughness to mica. Mica was treated using Hydrofluoric

Acid (HF) to form 1.0 nm deep etch pits, defined by the crystallographic structure of mica (Figure 7A). The etched mica has an order of magnitude larger  $R_a$  roughness than freshly cleaved mica, from  $0.029 \pm 0.002$  nm to  $0.26 \pm 0.01$  nm. Forming DPPC/DOPC (60:40) bilayers on etched mica produced much smaller domains than on flat mica (Figure 7B), with morphologies and correlation lengths (57nm) much closer to the domains on glass. The roughness is higher than glass, but with a lower spatial density, but nonetheless proves that as the surface is roughened, large scale domain formation is hindered.

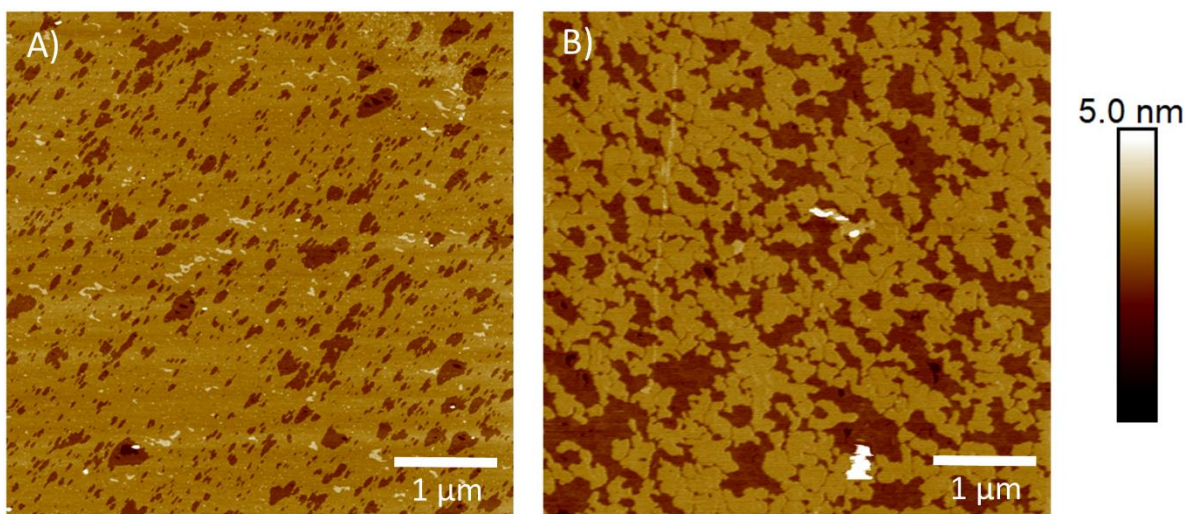


**Figure 7. AFM images of A) Mica etched in 40% HF for 30min, and B) DPPC/DOPC(60:40) bilayer on HF etched mica. Note - A and B are not the same area, but are on the same sample stub. Scale bars are shown on images and z scale is 5nm. RMS roughness of A is  $0.26 \pm 0.01$  nm. Correlation length of Domains in B is  $0.057 \mu\text{m}$  /57nm.**

## **Roughness affects Bilayer Structure**

We have shown a clear link between substrate roughness and domain size. Before we discuss the potential mechanisms for domain formation, the effect of roughness at different length scale on bilayer dynamics and structure must be discussed, in terms of both our results and literature.



Blachon et al. show how increasing the roughness of glass and silicon substrates from 0.1-3 nm using etching methods, decreases fluid phase bilayer diffusion 5 fold.<sup>50</sup> Goksu et al. also show reduction in diffusion on 0.71nm roughness silicon xerogels compared to mica.<sup>51</sup> The proposed mechanisms for this decrease in diffusion on rough surfaces are based on the observation that bilayers have been shown using AFM and Neutron Reflectometry to conform to the surface topography.<sup>50,52-54</sup> These mechanisms include curvature induced areas of ordered bilayer with slower diffusion coexisting with the bulk fluid phase to reduce average diffusion,<sup>50</sup> curvature induced holes if the curvature is too high (radius of curvature < 40nm) which restrict diffusion,<sup>50</sup> and also hidden area effects due to the vertical component of diffusion up and down the side of rough features.<sup>50,53</sup> Our roughness values of mica (0.029 nm) and glass (0.148 nm) extend the range lower than that investigated by Blachon et al (0.1-3 nm), and we see no reduction in diffusion between mica and glass.

AFM observations show that the top surface of bilayers are rougher on rougher glass and silicon compared to mica.<sup>12,41,51</sup> Course-grained molecular dynamics simulations show that molecular scale corrugations 0.3nm in height and width decrease the degree of periodic bilayer ordering.<sup>55</sup> Also our experiments showed that  $T_m$  and thus lipid ordering was reduced on rougher glass compared to mica. The lateral dimensions of surface roughness are also important. For 1-10 nm surface features, the bilayer does not simply follow the surface curvature,<sup>51</sup> and bilayers can span across pores that are less than twice the bilayer width (around 8-10nm).<sup>56</sup> This all suggests that if the roughness is a small percentage of the lipid bilayer height and the lateral separation between roughness peaks is small compared to bilayer dimensions, instead of curving to follow the corrugations of the surface and thus introducing diffusion reducing curvature effects, the roughness instead induces disorder in the bilayer.

## Roughness affects Domain Formation on Glass

There is a clear link between the micron scale fractal domains on smooth mica and the rough nanoscale domains on rougher glass. Glass is 4 times rougher than mica before bilayer deposition, and we have demonstrated that mica roughened on the nanoscale hinders domain growth with a length scale similar to glass. Lipid diffusion does not vary between the two substrates indicating that individual molecules are not hindered by the rougher surface. Slower cooling rates, allowing more time for the lipids to diffuse, does not result in larger domains on glass, whereas it does on mica. This suggests that the nanoscale roughness of the glass surface is somehow limiting the motion of structures above individual molecules, either clusters or small domains, and pinning them to a limiting length scale. This would also seem to be supported by the decades old observation of Radler et al. who showed that the spreading velocity of a bilayer is decreased by over an order of magnitude on glass compared to mica.<sup>57</sup> In other words, hydrodynamic flow of a bilayer is vastly slowed by the friction from a surface with a particular nanoscale roughness. Simulations by Ngamsaad et al. have shown that bilayers with asymmetric leaflet dynamics, as suggested in an SLB, result in restriction of domain growth to a limiting size,  $L_{pin}$ .<sup>58</sup> They model a phase-separating bilayer in which domains in the top leaflet can grow diffusively and by hydrodynamic flow, but only diffusively in the bottom leaflet. This mimics the restriction in hydrodynamic flow of a substrate surface on the bottom bilayer leaflet. An interleaflet coupling term then acts to pin domains across the two leaflets and limit the domains to a characteristic size, although it should be pointed out that we do not observe a difference in the upper-leaflet structure, implying that the two leaflets are strongly energetically coupled.

To summarise, as the bilayer is cooled from a homogenous single phase through the phase boundary to the two-phase region, the lipids become immiscible and the gel phase begins to nucleate out from the bulk fluid phase. There are now two possible mechanistic differences

between the two substrates. Firstly, there are many more domains on glass than mica, and this could be due to the roughness lowering the local activation energy for domain nucleation, providing more sites for nucleation than on mica. Secondly, the roughness of the substrate hinders domain ripening via coalescence of small clusters and domains (but not by molecular diffusion). This process could be due to two mechanisms. Rough surfaces can be highly curved. For a bilayer to map to a curved surface there is an interplay between positive Van der Waal interactions between the bilayer and the surface, and the bilayer bending penalty to follow the surface.<sup>32</sup> This energy penalty for bending is larger for the more tightly packed gel domains than fluid domains, and more ordered domains have been shown to colocalise to lower curvature regions in double supported bilayers and GUVs.<sup>19,20,34</sup> This could act to hinder the hydrodynamic flow of gel domains over highly curved substrate areas. It is likely that on glass the molecular scale roughness affects the molecular order of the bilayer shown through the slightly decreased  $T_m$ , and is not large enough to bring in curvature effects. A different, but related mechanism, would be the direct contact of lipid domains with high points on the rough surface, where the sharpness/curvature of the surface is too small for the bilayer to deflect around. This could also be mediated by the water layer, which is known to be structured to some degree, and hence the pinning point does not necessarily need to be in absolute contact with the surface peak. Once nucleation has commenced, the freely diffusing lipid on glass accrete around the many small nucleating clusters. As they grow into small domains they become stuck to the surface due to the restriction of hydrodynamic flow of domains, hindering further coalescence. On the smooth mica there is much less friction and the domains can grow larger, both by diffusion of lipids to growing domains and by flow and coalescence of smaller domains into larger ones.

As, touched upon above, an important parameter that must have an influence on the level of domain-substrate pinning is the thickness of the interstitial water layer. It is hard to measure the thickness of this layer between SLBs and substrates directly, with values stated to be between 0.3 and 2nm,<sup>32,50</sup> although our AFM measurements tend to indicate a depth of approximately 1 nm. Properties of this water layer can affect the spreading and flow of groups of lipid, for example by changing the pH.<sup>32</sup> It is likely that the structure and dynamics of the interstitial water layer vary between mica and glass due to the surface topography i.e. roughness, but also due to electrostatics and surface chemistry. The thickness of the interstitial water layer along with structure and dynamics could be having dramatic effects on the hydrodynamic flow of lipids and domains. It is likely that the effect of roughness on lipid flow is the combination of the mechanisms described above, and further study is needed to isolate their different effects.

## **Formation of Optically Visible Domains on Glass**

As shown in Figure 1, domains on glass that are beyond the resolution of traditional microscopy are clearly visible using AFM. This is likely why there is a disproportionately small number of publications purporting to show phase separating systems on glass, compared for example to the ubiquitous phase separation in GUVs and supported bilayers on mica. It has likely been tried by many researchers who have assumed that no domains have formed and thus not published, when in fact the domains were likely forming but were not observed by lower resolution techniques. Of the published work looking at phase separated systems on glass, we only found one paper by Honigmann et al. showing similar nanoscale domains on glass.<sup>8</sup> Using DPPC/DPhPC/Chol SLBs they observed distinct micron scale liquid-liquid ( $L_o$ - $L_d$ ) domains on mica using fluorescence. The same lipid system on glass however only showed unclear phase separation, not fully resolvable due to the diffraction limit. A combination of STED and STED-FCS, enabling super resolution,

confirmed the presence nanoscale domains ranging from 40-300nm with an average of 90nm. The study complements ours, by showing that the nanoscale domains formed on glass occur for liquid-liquid phase separating systems as well as gel-liquid systems. Seu et al. and Burns et al. show domains on glass with DPPC/DOPC and DPPC/DOPC/Chol systems respectively that do not match with any domains we have observed in similar systems, or with domains observed by Honigmann et al.<sup>8</sup> The reason for this discrepancy is unknown. Based on examples in the literature, silicon substrates with roughness values matching those of glass, seem to also hinder the formation of phase separating systems of phospholipid/glycolipid<sup>59</sup> and phospholipid/protein,<sup>60</sup> compared to the same systems on mica. Reports of domains on silicon substrates in the literature are also rare, as with on glass.

Visible domains have been observed in GUVs deposited onto glass substrates, if domains were already present in the GUVs before deposition.<sup>13,25,30</sup> These domains do not reform on temperature cycling to sufficiently high temperatures,<sup>13,25</sup> but a ‘speckle’ pattern is observed.<sup>13</sup> From our AFM studies of bilayers on glass, we can explain these results. Pre-formed micron size domains in GUVs are not hindered in growth by the substrate as they have already formed. Once they are raised sufficiently above the miscibility transition temperature the lipids are mixed homogeneously. When the lipids are cooled and become immiscible again, the presence of the glass surface hinders the growth of domains and results in a ‘speckle’ pattern of domains just below the optical resolution. Similarly, Langmuir-Blodgett/Langmuir Schaefer bilayers formed on glass show phase separation, provided there was phase separation in the initial monolayers before deposition.<sup>13,28</sup> Again when the temperature is cycled these domains do not re-form but a ‘speckle’ pattern is observed.<sup>13</sup>

## Substrates Decoupling Effects

SLB substrates can potentially affect the proximal (bottom) leaflet more than the distal (top) leaflet, resulting in decoupling of physical properties. Recent Single-Particle Tracking (SPT) experiments have shown two separate diffusion coefficients for a DOPC bilayer on glass, the slower attributed to the proximal bilayer leaflet.<sup>33</sup> FCS Experiments of DOPC show no clear decoupling of the two leaflets on mica or glass,<sup>2,9</sup> but another recent FCS study shows decoupling of DOPC on glass when a fluorescence quencher is used to isolate the two leaflets.<sup>61</sup> Several studies have also shown that decoupling of leaflet dynamics may be substrate dependent with decoupling on mica but not glass or silica.<sup>10,41</sup>

Lipid dyes may be excluded from the proximal leaflet of a SLB, due to steric constraints with the surface or the more tightly packed proximal leaflet. Based on Fluorescence Interference Contrast Microscopy (FLIC) and Fluorescence Quenching experiments, the TR-DHPE dye is likely partitioning 70-78% into the distal bilayer leaflet in our fluid lipid system, and the NBD 16:0 PE 50:50 between the two leaflets.<sup>40,62</sup> We therefore observe an average of the two leaflets when measuring diffusion, and are unable to discern if there is dynamic asymmetry for our experimental setup. We note that diffusion decoupling is possible and further studies may link asymmetric dynamics to domain formation.

Decoupling of the leaflet melting transitions ( $T_m$ ) have also been reported multiple times for SLBs on mica by AFM, the results summed up nicely by Giocondi et al. .<sup>27,35</sup> The  $T_m$  transitions are broad with the lower of the two decoupled transitions between 41-52 °C and the higher between 46.5-60 °C. The values from the different studies vary significantly within these ranges, with the lower range just above the  $T_m$  of MLVs. DSC of DPPC supported on mica chips also shows two transitions but closer together at 42.4 °C and 44.8 °C.<sup>63</sup>

Conversely, in this study only one transition is observed on mica and glass up to a temperature of 55 °C, which is above the onset of all upper temperature decoupled transitions reported. The dyes are present in both leaflets, so we should be able to observe decoupling of  $T_m$  if it is occurring. For both mica and glass the fluorescence did not show partial recovery during the transition, which would be indicative of one leaflet crystallising and its diffusion dropping earlier than the other. Instead they showed close to total recovery above  $T_m$  and close to no recovery below, meaning both leaflets have gone through the transition. Literature FRAP-with-temperature studies show similar results with no decoupling of  $T_m$ .<sup>10,42,44</sup> Also, on mica DPPC crystallises from liquid to gel excluding the dye in a single event, not two (Figure S4). Both the crystallisation and the growth are coupled across the leaflets.

This discrepancy in results points to a problem with some techniques, with the preparation techniques or in the interpretation of data that arise. Some of the wide variation in molecular diffusion rates could indicate that the probe molecule being measured is not purely reporting on the state of the adjacent bilayer, but also to the probes own interaction with the substrate or interstitial water later, possibly via a differential response to the surface roughness, and it does not precisely report the absolute lipid diffusion rate. Similarly, if particle tracking is used to discriminate between diffusion in proximal and distal leaflets, it might also be reporting on the interaction between the particle and substrate/interstitial layer.

## Conclusion

We have shown that nanoscale domains form on glass, in lipid mixtures that form micron scale domains on mica and in GUVs. These domains have likely not been observed before due to the domains being below the resolution of diffraction limited optics. Molecular diffusion is not affected by the different surfaces, but hydrodynamic flow of groups of lipids and domains is

hindered on glass, preventing formation of micron scale domains. We have shown a link between the micron scale domains forming on molecular smooth mica and hindered domain formation on rough glass, as well as hindered domain formation on mica roughened on the nanoscale. Blachon et al have shown how increasing substrate roughness of silicon and glass using etching between 0.1-3nm reduces bilayer diffusion 5-fold. For commonly used bilayer substrates with common preparation procedures, such as piranha cleaned glass and cleaved mica, the roughness values are 0.148 nm and 0.029 nm. We have shown that at this scale molecular diffusion is not affected by the substrate. This is likely due to roughness being too low compared to bilayer dimensions, both vertically and laterally, for the bilayer to conform to the surface and introduce diffusion reducing curvature effects. Instead we have shown that hydrodynamic flow of groups of lipids and domains is hindered on rough glass, preventing formation of micron scale domains. We are also interested in how electrostatics may affect domain formation as they affect many bilayer properties,<sup>42</sup> but this is not discussed here.

Although glass is used ubiquitously for optical imaging purposes, it requires cleaning in harsh chemicals to render it clean enough and hydrophilic enough to support lipid bilayers, and after this treatment the surface is still molecularly rough and heterogeneous. Mica in comparison, can be cleaved in a matter of seconds using tape/tweezers/scalpel, leaving a clean, hydrophilic and atomically flat surface. Mica is commonly used as an AFM substrate, but high-quality optical images of bilayers can also be obtained through mica.

Decoupling of diffusion or  $T_m$  between the two bilayer leaflets was not observed in our study, but both have been observed in the literature. There is still much to understand regarding asymmetry in physical bilayer properties, coupling between the two leaflets, how asymmetry and coupling link to domain formation and how all of this is affected by different substrates. In vivo



the cytoskeleton, a dense layer of action filaments which is pinned to the membrane by protein interactions, can potentially provide asymmetry and act to restrict domain growth. Macroscopic optically resolvable phase separation is not observable in the plasma membrane of cultured mammalian cells, but is observable in cytoskeleton-free Giant Plasma Membrane Vesicle (GPMVs) induced from these same cells.<sup>64,65</sup> Pinning a minimal cytoskeleton to a phase separating SLB restricts the growth of micron scale domains and when the pinning sites are in both the  $L_o$  and the  $L_d$  phase, the nanoscale phase structure is strikingly similar to the phase separation we see on glass.<sup>15</sup> Experiments with GUVs,<sup>66</sup> as well as simulations,<sup>67-69</sup> also show how cytoskeleton-like pinning sites can restrict large scale domains formation. This all provides strong evidence that the presence of the cytoskeleton is a factor in restricting macroscopic phase separation, and also potentially providing sites for domain nucleation. This supports the idea that substrates may be a more accurate model for in vivo membranes than free-floating membranes. As the membrane biophysics community search for more accurate and controllable models for the cell membrane it is important to try to replicate the effects of the polymeric networks of extracellular matrix and actin cortex.

## Associated Content

The supporting information includes figures on domain size and correlation length methods (S1-S2), combined AFM and fluorescence of domains (S3), nucleation of the DPPC + 0.5mol% TR DHPE domains shown in Figure 4 (S4), a wider set of DPPC/DOPC (60:40) AFM images (S5), AFM images of nanoholes in glass substrates (S6-S7) and FRAP-with-temperature raw images (S8).

## Author Information

Corresponding Author

\*s.d.a.connell@leeds.ac.uk

## Acknowledgment

The work was supported by EPSRC grant EP/J017566/1 ‘CAPITALS’. We acknowledge Dr Peng Bao and Sophie Meredith for help with Fluorescence and FRAP measurements, and Dr Mark Tarn for the HF acid etch.

## References

- (1) Schmidt, M. L.; Ziani, L.; Boudreau, M.; Davis, J. H. Phase Equilibria in DOPC/DPPC: Conversion from Gel to Subgel in Two Component Mixtures. *J. Chem. Phys.* **2009**, *131* (175103).
- (2) Przybylo, M.; Sýkora, J.; Humpolíčová, J.; Benda, A.; Zan, A.; Hof, M. Lipid Diffusion in Giant Unilamellar Vesicles Is More than 2 Times Faster than in Supported Phospholipid Bilayers under Identical Conditions. *Langmuir* **2006**, *22*, 9096–9099.
- (3) Biltonen, R. L.; Lichtenberg, D. The Use of Differential Scanning Calorimetry as a Tool to Characterize Liposome Preparations. *Chem. Phys. Lipids* **1993**, *64* (1–3), 129–142.
- (4) Mazur, F.; Bally, M.; Städler, B.; Chandrawati, R. Liposomes and Lipid Bilayers in Biosensors. *Adv. Colloid Interface Sci.* **2017**, *249*, 88–99.
- (5) Pattni, B. S.; Chupin, V. V.; Torchilin, V. P. New Developments in Liposomal Drug Delivery. *Chem. Rev.* **2015**, *115* (19), 10938–10966.
- (6) Connell, S. D.; Smith, D. A. The Atomic Force Microscope as a Tool for Studying Phase Separation in Lipid Membranes. *Mol. Membr. Biol.* **2006**, *23* (1), 17–28.

- (7) Richter, R. P.; Brisson, A. R. Following the Formation of Supported Lipid Bilayers on Mica: A Study Combining AFM, QCM-D, and Ellipsometry. *Biophys. J.* **2005**, *88* (5), 3422–3433.
- (8) Honigmann, A.; Mueller, V.; Hell, S. W.; Eggeling, C. STED Microscopy Detects and Quantifies Liquid Phase Separation in Lipid Membranes Using a New Far-Red Emitting Fluorescent Phosphoglycerolipid Analogue. *Faraday Discuss.* **2013**, *161*, 77–89.
- (9) Benda, A.; Beneš, M.; Mareček, V.; Lhotský, A.; Hermens, W. T.; Hof, M. How to Determine Diffusion Coefficients in Planar Phospholipid Systems by Confocal Fluorescence Correlation Spectroscopy. *Langmuir* **2003**, *19* (10), 4120–4126.
- (10) Scomparin, C.; Lecuyer, S.; Ferreira, M.; Charitat, T.; Tinland, B. Diffusion in Supported Lipid Bilayers: Influence of Substrate and Preparation Technique on the Internal Dynamics. *Eur. Phys. J. E* **2009**, *28* (2), 211–220.
- (11) Seu, K. J.; Pandey, A. P.; Haque, F.; Proctor, E. A.; Ribbe, A. E.; Hovis, J. S. Effect of Surface Treatment on Diffusion and Domain Formation in Supported Lipid Bilayers. *Biophys. J.* **2007**, *92* (7), 2445–2450.
- (12) Chada, N.; Sigdel, K. P.; Sanganna Gari, R. R.; Matin, T. R.; Randall, L. L.; King, G. M. Glass Is a Viable Substrate for Precision Force Microscopy of Membrane Proteins. *Sci. Rep.* **2015**, *5*, 1–8.
- (13) Stottrup, B. L.; Veatch, S. L.; Keller, S. L. Nonequilibrium Behavior in Supported Lipid Membranes Containing Cholesterol. *Biophys. J.* **2004**, *86* (5), 2942–2950.
- (14) Heath, G. R.; Johnson, B. R. G.; Olmsted, P. D.; Connell, S. D.; Evans, S. D. Actin Assembly at Model-Supported Lipid Bilayers. *Biophys. J.* **2013**, *105* (10), 2355–2365.

- (15) Honigmann, A.; Sadeghi, S.; Keller, J.; Hell, S. W.; Eggeling, C.; Vink, R. A Lipid Bound Actin Meshwork Organizes Liquid Phase Separation in Model Membranes. *Elife* **2014**, *2014* (3), 1–16.
- (16) Sonnleitner, A.; Schütz, G. J.; Schmidt, T. Free Brownian Motion of Individual Lipid Molecules in Biomembranes. *Biophys. J.* **1999**, *77* (5), 2638–2642.
- (17) Sezgin, E.; Levental, I.; Mayor, S.; Eggeling, C. The Mystery of Membrane Organization: Composition, Regulation and Roles of Lipid Rafts. *Nat. Rev. Mol. Cell Biol.* **2017**, *18* (6), 361–374.
- (18) Jensen, M. H.; Morris, E. J.; Simonsen, A. C. Domain Shapes, Coarsening, and Random Patterns in Ternary Membranes. *Langmuir* **2007**, *23* (12), 8135–8141.
- (19) Subramaniam, A. B.; Lecuyer, S.; Ramamurthi, K. S.; Losick, R.; Stone, H. A. Particle/Fluid Interface Replication as a Means of Producing Topographically Patterned Polydimethylsiloxane Surfaces for Deposition of Lipid Bilayers. *Adv. Mater.* **2010**, *22* (19), 2142–2147.
- (20) Parthasarathy, R.; Yu, C.; Groves, J. T. Curvature-Modulated Phase Separation in Lipid Bilayer Membranes. *Langmuir* **2006**, *22* (11), 5095–5099.
- (21) Jackman, J.; Knoll, W.; Cho, N.-J. Biotechnology Applications of Tethered Lipid Bilayer Membranes. *Materials (Basel)*. **2012**, *5* (12), 2637–2657.
- (22) Tanaka, M.; Sackmann, E. Polymer-Supported Membranes as Models of the Cell Surface. *Nature* **2005**, *437* (7059), 656–663.

- (23) Connell, S. D.; Heath, G.; Olmsted, P. D.; Kisil, A. Critical Point Fluctuations in Supported Lipid Membranes. *Faraday Discuss.* **2013**, *161*, 91.
- (24) Aufderhorst-Roberts, A.; Chandra, U.; Connell, S. D. Three-Phase Coexistence in Lipid Membranes. *Biophys. J.* **2017**, *112* (2), 313–324.
- (25) Gunderson, R. S.; Honerkamp-Smith, A. R. Liquid-Liquid Phase Transition Temperatures Increase When Lipid Bilayers Are Supported on Glass. *Biochim. Biophys. Acta - Biomembr.* **2018**, *1860* (10), 1965–1971.
- (26) Bernchou, U.; Ipsen, J. H.; Simonsen, A. C. Growth of Solid Domains in Model Membranes : Quantitative Image Analysis Reveals a Strong Correlation between Domain Shape and Spatial Position. *J. Phys. Chem.* **2009**, *113*, 7170–7177.
- (27) Alessandrini, A.; Facci, P. Phase Transitions in Supported Lipid Bilayers Studied by AFM. *Soft Matter* **2014**, *10* (37), 7145–7164.
- (28) Dietrich, C.; Bagatolli, L. A.; Volovyk, Z. N.; Thompson, N. L.; Levi, M.; Jacobson, K.; Gratton, E. Lipid Rafts Reconstituted in Model Membranes. *Biophys. J.* **2001**, *80* (3), 1417–1428.
- (29) Crane, J. M.; Tamm, L. K. Role of Cholesterol in the Formation and Nature of Lipid Rafts in Planar and Spherical Model Membranes. *Biophys. J.* **2004**, *86* (5), 2965–2979.
- (30) Kaizuka, Y.; Groves, J. T. Structure and Dynamics of Supported Intermembrane Junctions. *Biophys. J.* **2004**, *86* (2), 905–912.
- (31) Burns, A. R.; Frankel, D. J.; Buranda, T. Local Mobility in Lipid Domains of Supported Bilayers Characterized by Atomic Force Microscopy and Fluorescence Correlation Spectroscopy. *Biophys. J.* **2005**, *89* (2), 1081–1093.

- (32) Cremer, P. S.; Boxer, S. G. Formation and Spreading of Lipid Bilayers on Planar Glass Supports. *J. Phys. Chem. B* **1999**, *103* (13), 2554–2559.
- (33) Schoch, R. L.; Barel, I.; Brown, F. L. H.; Haran, G. Lipid Diffusion in the Distal and Proximal Leaflets of Supported Lipid Bilayer Membranes Studied by Single Particle Tracking. *J. Chem. Phys.* **2018**, *148* (12), 123333.
- (34) Baumgart, T.; Hess, S. T.; Webb, W. W. Imaging Coexisting Fluid Domains in Biomembrane Models Coupling Curvature and Line Tension. *Nature* **2003**, *425*, 821–824.
- (35) Giocondi, M. C.; Yamamoto, D.; Lesniewska, E.; Milhiet, P. E.; Ando, T.; Le Grimellec, C. Surface Topography of Membrane Domains. *Biochim. Biophys. Acta - Biomembr.* **2010**, *1798* (4), 703–718.
- (36) Nagahara, L. A.; Hashimoto, K.; Fujishima, A.; Snowden-Ifft, D.; Price, P. B. Mica Etch Pits as a Height Calibration Source for Atomic Force Microscopy. *J. Vac. Sci. Technol. B Microelectron. Nanom. Struct.* **1994**, *12* (3), 1694.
- (37) Lentz, B. R.; Barenholz, Y.; Thompson, T. E. Fluorescence Depolarization Studies of Phase Transitions and Fluidity in Phospholipid Bilayers. 2 Two-Component Phosphatidylcholine Liposomes. *Biochemistry* **1976**, *15* (20), 4529–4537.
- (38) Honerkamp-Smith, A. R.; Veatch, S. L.; Keller, S. L. An Introduction to Critical Points for Biophysicists; Observations of Compositional Heterogeneity in Lipid Membranes. *Biochim. Biophys. Acta - Biomembr.* **2009**, *1788* (1), 53–63.

- (39) McKiernan, A. E.; Ratto, T. V.; Longo, M. L. Domain Growth, Shapes, and Topology in Cationic Lipid Bilayers on Mica by Fluorescence and Atomic Force Microscopy. *Biophys. J.* **2000**, *79* (5), 2605–2615.
- (40) Crane, J. M.; Kiessling, V.; Tamm, L. K. Measuring Lipid Asymmetry in Planar Supported Bilayers by Fluorescence Interference Contrast Microscopy. *Langmuir* **2005**, *21* (4), 1377–1388.
- (41) Motegi, T.; Yamazaki, K.; Ogino, T.; Tero, R. Substrate-Induced Structure and Molecular Dynamics in a Lipid Bilayer Membrane. *Langmuir* **2017**, *33* (51), 14748–14755.
- (42) Harb, F. F.; Tinland, B. Effect of Ionic Strength on Dynamics of Supported Phosphatidylcholine Lipid Bilayer Revealed by FRAP and Langmuir-Blodgett Transfer Ratios. *Langmuir* **2013**, *29* (18), 5540–5546.
- (43) Attwood, S. J.; Choi, Y.; Leonenko, Z. Preparation of DOPC and DPPC Supported Planar Lipid Bilayers for Atomic Force Microscopy and Atomic Force Spectroscopy. *Int. J. Mol. Sci.* **2013**, *14* (2), 3514–3539.
- (44) Tamm, L. K.; McConnell, H. M. Supported Phospholipid Bilayers. *Biophys. J.* **1985**, *47* (1), 105–113.
- (45) Ali, S.; Minchey, S.; Janoff, A.; Mayhew, E. A Differential Scanning Calorimetry Study of Phosphocholines Mixed with Paclitaxel and Its Bromoacylated Taxanes. *Biophys. J.* **2000**, *78* (1), 246–256.
- (46) Naumann, C.; Brumm, T.; Bayerl, T. M. Phase Transition Behavior of Single Phosphatidylcholine Bilayers on a Solid Spherical Support Studied by DSC, NMR and FT-IR. *Biophys. J.* **1992**, *63* (5), 1314–1319.

- (47) Lewis, R. N.; Mannock, D. A.; McElhaney, R. N. Differential Scanning Calorimetry in the Study of Lipid Phase Transitions in Model and Biological Membranes: Practical Considerations. In *Methods Mol.Biol.*; 2007; Vol. 400, pp 171–195.
- (48) Bao, P.; Cartron, M. L.; Sheikh, K. H.; Johnson, B. R. G.; Hunter, C. N.; Evans, S. D. SI - Controlling Transmembrane Protein Concentration and Orientation in Supported Lipid Bilayers. *Chem. Commun.* **2017**, 53 (30), 4250–4253.
- (49) Richter, R. P.; Escarpit, R. R.; Cedex, P. Formation of Solid-Supported Lipid Bilayers : An Integrated View. *Langmuir* **2006**, 22 (8), 3497–3505.
- (50) Blachon, F.; Harb, F.; Munteanu, B.; Piednoir, A.; Fulcrand, R.; Charitat, T.; Fragneto, G.; Pierre-Louis, O.; Tinland, B.; Rieu, J. P. Nanoroughness Strongly Impacts Lipid Mobility in Supported Membranes. *Langmuir* **2017**, 33 (9), 2444–2453.
- (51) Goksu, E. I.; Hoopes, M. I.; Nellis, B. A.; Xing, C.; Faller, R.; Frank, C. W.; Risbud, S. H.; Satcher, J. H.; Longo, M. L. Silica Xerogel/Aerogel-Supported Lipid Bilayers: Consequences of Surface Corrugation. *Biochim. Biophys. Acta - Biomembr.* **2010**, 1798 (4), 719–729.
- (52) Goksu, E. I.; Vanegas, J. M.; Blanchette, C. D.; Lin, W.-C.; Longo, M. L. AFM for Structure and Dynamics of Biomembranes. *Biochim. Biophys. Acta* **2009**, 1788 (1), 254–266.
- (53) Werner, J. H.; Montan, G. A.; Garcia, A. L.; Zurek, N. A.; Akhadov, E. A.; Lopez, G. P.; Shreve, A. P. Formation and Dynamics of Supported Phospholipid Membranes on a Periodic Nanotextured Substrate Formation and Dynamics of Supported Phospholipid Membranes on a Periodic Nanotextured Substrate. *Langmuir* **2009**, No. 25, 2986–2993.

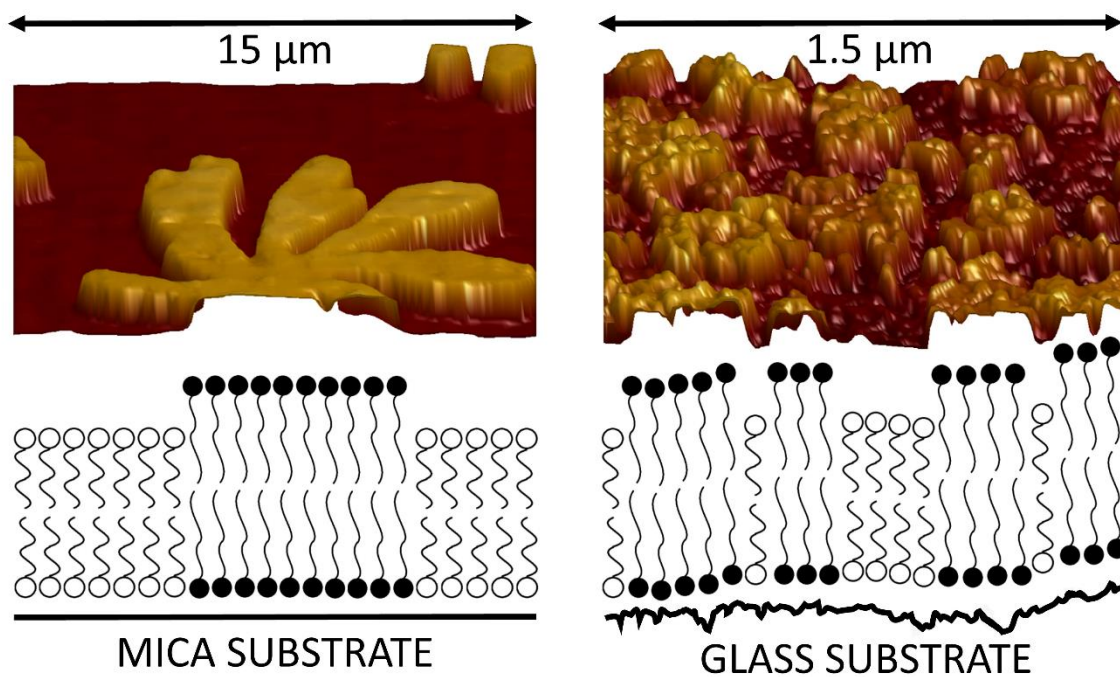


- (54) Sanii, B.; Smith, A. M.; Butti, R.; Brozell, A. M.; Parikh, A. N. Bending Membranes on Demand: Fluid Phospholipid Bilayers on Topographically Deformable Substrates. *Nano Lett.* **2008**, *8* (3), 866–871.
- (55) Xing, C.; Faller, R. Interactions of Lipid Bilayers with Supports: A Coarse-Grained Molecular Simulation Study. *J. Phys. Chem. B* **2008**, *112* (23), 7086–7094.
- (56) Davis, R. W.; Flores, A.; Barrick, T. A.; Cox, J. M.; Brozik, S. M.; Lopez, G. P.; Brozik, J. A. Nanoporous Microbead Supported Bilayers: Stability, Physical Characterization, and Incorporation of Functional Transmembrane Proteins. *Langmuir* **2007**, *23* (7), 3864–3872.
- (57) Rädler, J.; Strey, H.; Sackmann, E. Phenomenology and Kinetics of Lipid Bilayer Spreading on Hydrophilic Surfaces. *Langmuir* **1995**, *11* (11), 4539–4548.
- (58) Ngamsaad, W.; May, S.; Wagner, A. J.; Triampo, W. Pinning of Domains for Fluid–fluid Phase Separation in Lipid Bilayers with Asymmetric Dynamics. *Soft Matter* **2011**, *7* (6), 2848.
- (59) Lei, S. B.; Tero, R.; Misawa, N.; Yamamura, S.; Wan, L. J.; Urisu, T. AFM Characterization of Gramicidin-A in Tethered Lipid Membrane on Silicon Surface. *Chem. Phys. Lett.* **2006**, *429* (1–3), 244–249.
- (60) Mao, Y.; Shang, Z.; Imai, Y.; Hoshino, T.; Tero, R.; Tanaka, M.; Yamamoto, N.; Yanagisawa, K.; Urisu, T. Surface-Induced Phase Separation of a Sphingomyelin/Cholesterol/Ganglioside GM1-Planar Bilayer on Mica Surfaces and Microdomain Molecular Conformation That Accelerates A $\beta$  Oligomerization. *Biochim. Biophys. Acta - Biomembr.* **2010**, *1798* (6), 1090–1099.

- (61) Otsu, T.; Yamaguchi, S. Quantifying the Diffusion of Lipids in the Proximal/Distal Leaflets of a Supported Lipid Bilayer by Two-Dimensional Fluorescence Lifetime Correlation Spectroscopy. *J. Phys. Chem. B* **2018**, *122* (45), 10315–10319.
- (62) Ajo-Franklin, C. M.; Yoshina-Ishii, C.; Boxer, S. G. Probing the Structure of Supported Membranes and Tethered Oligonucleotides by Fluorescence Interference Contrast Microscopy. *Langmuir* **2005**, *21* (11), 4976–4983.
- (63) Yang, J.; Appleyard, J. The Main Phase Transition of Mica-Supported Phosphatidylcholine Membranes. *J. Phys. Chem. B* **2000**, *104* (34), 8097–8100.
- (64) Baumgart, T.; Hammond, A. T.; Sengupta, P.; Hess, S. T.; Holowka, D. A.; Baird, B. A.; Webb, W. W. Large-Scale Fluid/Fluid Phase Separation of Proteins and Lipids in Giant Plasma Membrane Vesicles. *Proc. Natl. Acad. Sci.* **2007**, *104* (9), 3165–3170.
- (65) Cornell, C. E.; Skinkle, A. D.; He, S.; Levental, I.; Levental, K. R.; Keller, S. L. Tuning Length Scales of Small Domains in Cell-Derived Membranes and Synthetic Model Membranes. *Biophys. J.* **2018**, *115* (4), 690–701.
- (66) Arumugam, S.; Petrov, E. P.; Schwille, P. Cytoskeletal Pinning Controls Phase Separation in Multicomponent Lipid Membranes. *Biophys. J.* **2015**, *108* (5), 1104–1113.
- (67) Yethiraj, A.; Weisshaar, J. C. Why Are Lipid Rafts Not Observed in Vivo? *Biophys. J.* **2007**, *93* (9), 3113–3119.
- (68) Machta, B. B.; Papanikolaou, S.; Sethna, J. P.; Veatch, S. L. Minimal Model of Plasma Membrane Heterogeneity Requires Coupling Cortical Actin to Criticality. *Biophys. J.* **2011**, *100* (7), 1668–1677.

(69) Fischer, T.; Vink, R. L. C. Domain Formation in Membranes with Quenched Protein Obstacles: Lateral Heterogeneity and the Connection to Universality Classes. *J. Chem. Phys.* **2011**, *134* (055106).

## For Table of Contents only



# Substrate Roughness Significantly affects Bilayer Phase Separation: A Comparison of Mica and Glass

Supporting Information

James A. Goodchild, Danielle L. Walsh and Simon D. Connell\*

School of Physics and Astronomy, University of Leeds, UK

\*[s.d.a.connell@leeds.ac.uk](mailto:s.d.a.connell@leeds.ac.uk)

Figure S1. Binary image of gel and liquid domains. Gel domains fitted to ellipses to determine size.

Figure S2. Correlation Length Analysis.

Figure S3. DPPC/DOPC (60:40) supported lipid bilayers on mica, imaged using both fluorescence and AFM on the same area using a combined AFM/Fluorescence microscope.

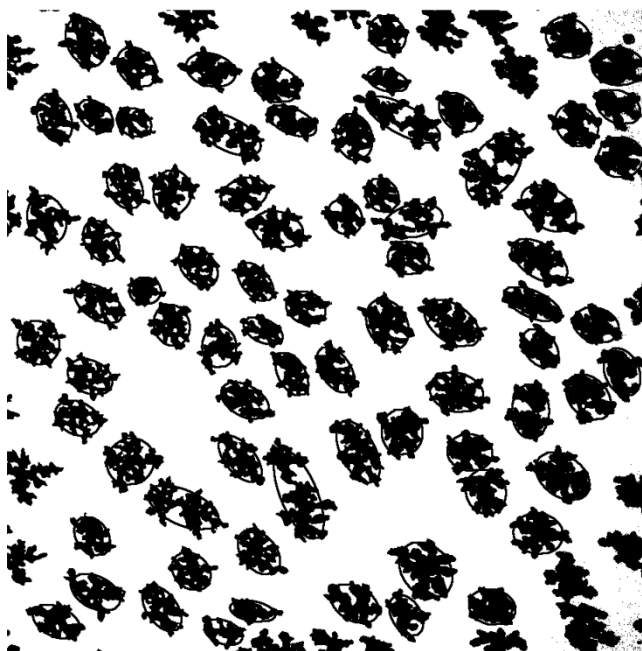
Figure S4. DPPC + 0.5mol% TR DHPE cooling through DPPC's transition temperature.

Figure S5. AFM images of DPPC/DOPC (60:40) on glass, 5 $\mu$ m and 20 $\mu$ m.

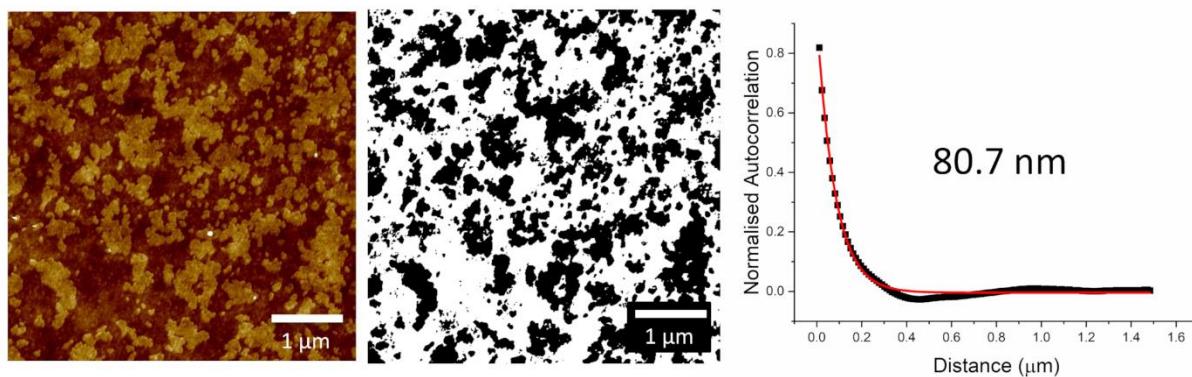
Figure S6. AFM images of glass substrate with nanoholes, and with DPPC/DOPC (60:40) bilayer on nanoholes

Figure S7. Nanoholes on glass substrates from our lab and from literature

Figure S8. FRAP on DPPC+ 0.5mol% NBD bilayer on glass as the bilayer cools raw images.



**Figure S1. Binary image of gel and liquid domains. Gel domains fitted to ellipses to determine size.**



**Figure S2. Correlation Length Analysis. AFM image showing gel and liquid phases on glass. Binary Image of two phases. Autocorrelation curve with exponential decay fit to calculate correlation length, correlation length displayed on graph.**

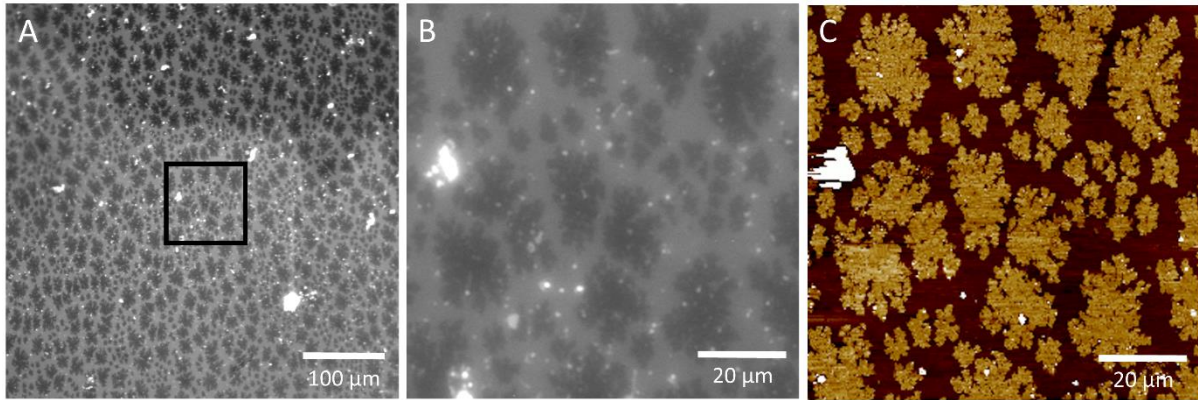


**Figure S3. DPPC/DOPC (60:40) supported lipid bilayers on mica, imaged using both fluorescence (A and B) and AFM (C) on the same area using a combined AFM/Fluorescence microscope. B is a separate image from A taken at a higher magnification. B and C are the same area as the black box in A. Z Scale of C is 3.5 nm. The white specks in the images correspond to lipid vesicles and aggregates stuck to the bilayer surface. The two different populations of domain size present in these images (large 20μm domains and small 5μm domains) demonstrates the effects of a non-controlled faster cool on domain formation. Domains nucleate and grow large but as the solution becomes super-saturated smaller domains crash out.**



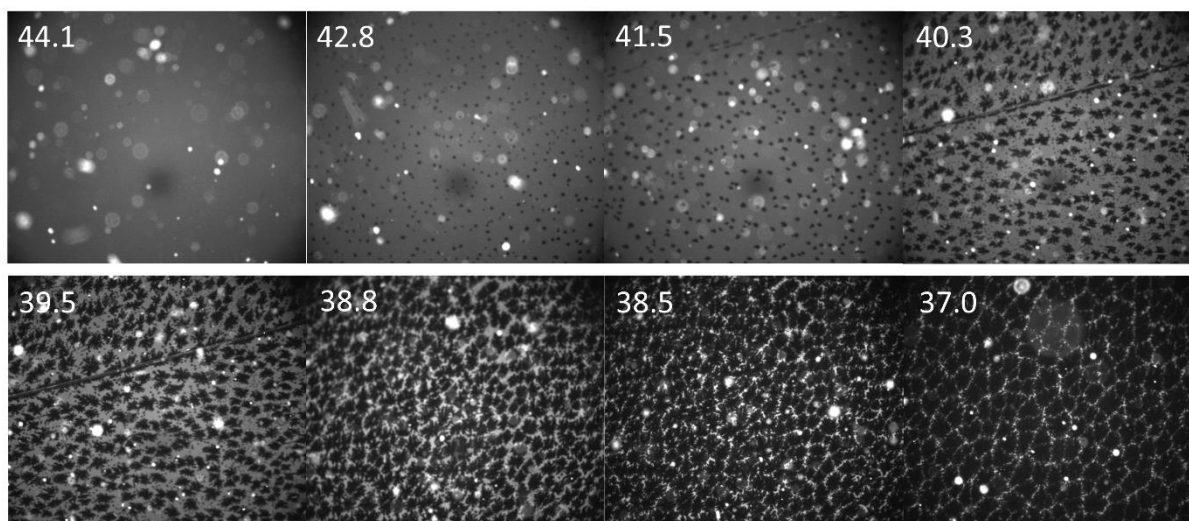


**Figure S4. DPPC + 0.5mol% TR DHPE cooling through DPPC's transition temperature. The bilayer is initially homogenous in the fluid phase. As the bilayer cools nucleation of pure DPPC domains excludes TR-DHPE dye.**

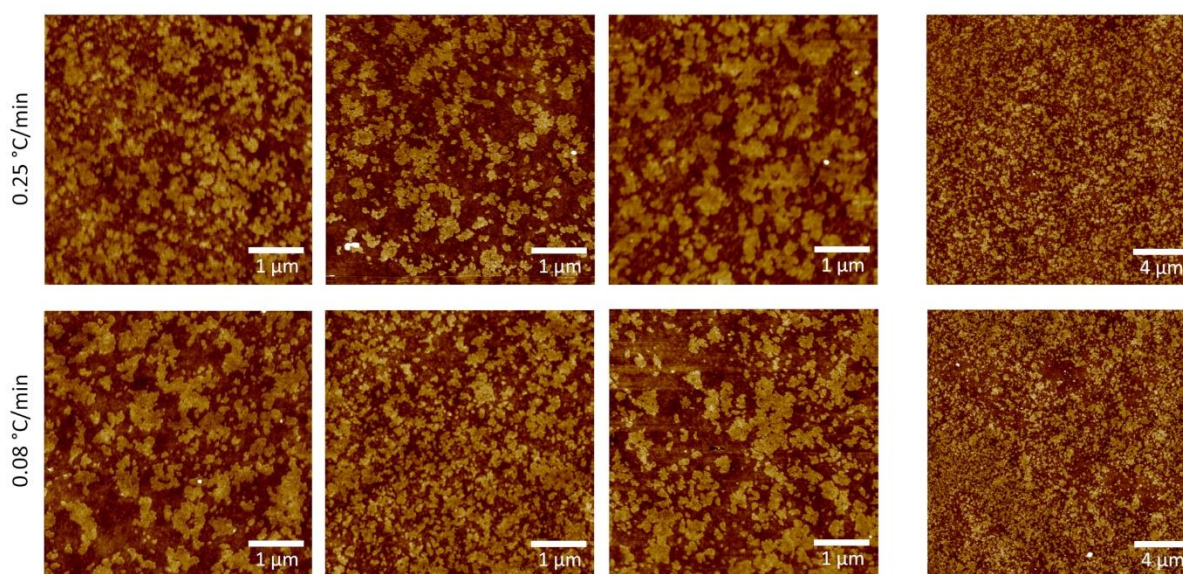


**Figure S5. AFM images of DPPC/DOPC (60:40) on glass, 5μm and 20μm. Images show heterogeneity in different areas of the substrates, and how a similar range of sizes, morphologies and clustering are seen with both the ambient (0.25°C/min) and slow (0.08°C/min) cool.**

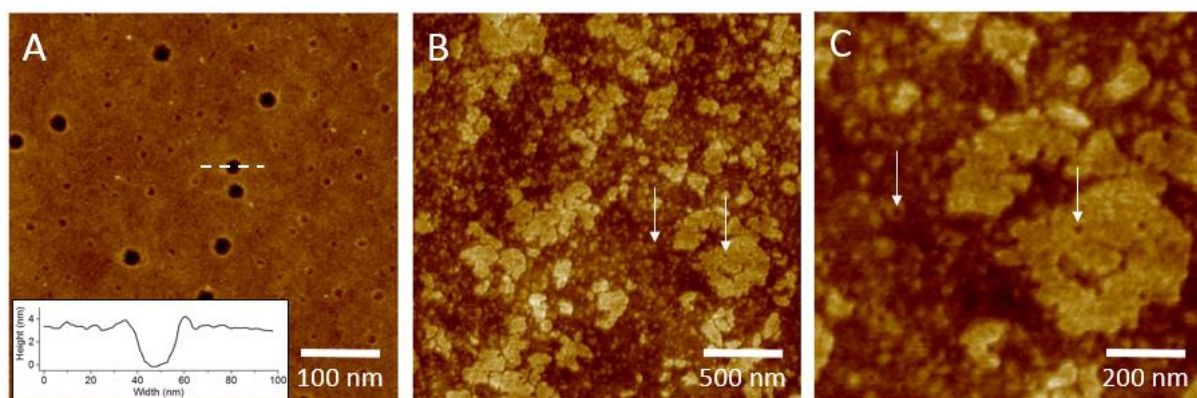


**Figure S6. AFM images of A) Glass substrate before Piranha/UV Ozone with nanoholes B) DPPC/DOPC (60:40) bilayer on glass, where nanoholes are visible in the bilayer at the same size as holes in the substrate (Note – different glass stubs in A and B) C) Zoom in of B, showing the nanoholes more clearly. Z scales of A is 8nm, B and C are 4nm.**

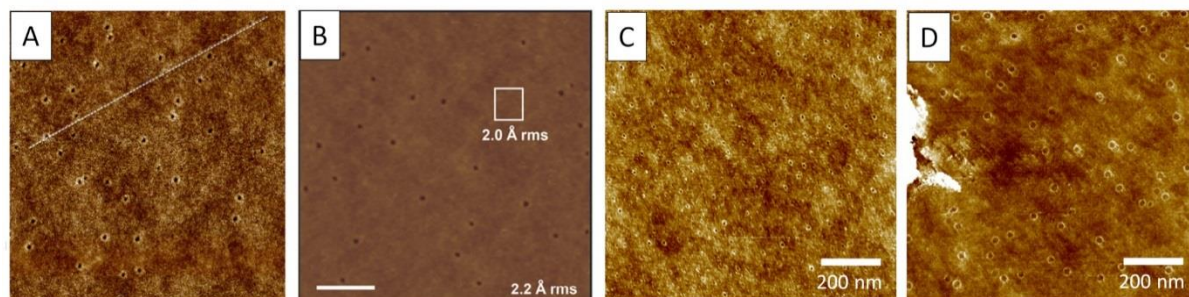


**Figure S7. Nanoholes on glass substrates A) From Bao 2017 B) From Chada 2015 C) and D) Different glass slides showing different distributions of nanoholes. Z Scale of a is 4nm, Z scale of b is 12nm, Z scales for c and D are 3nm. All images are 1μm<sup>2</sup>.**



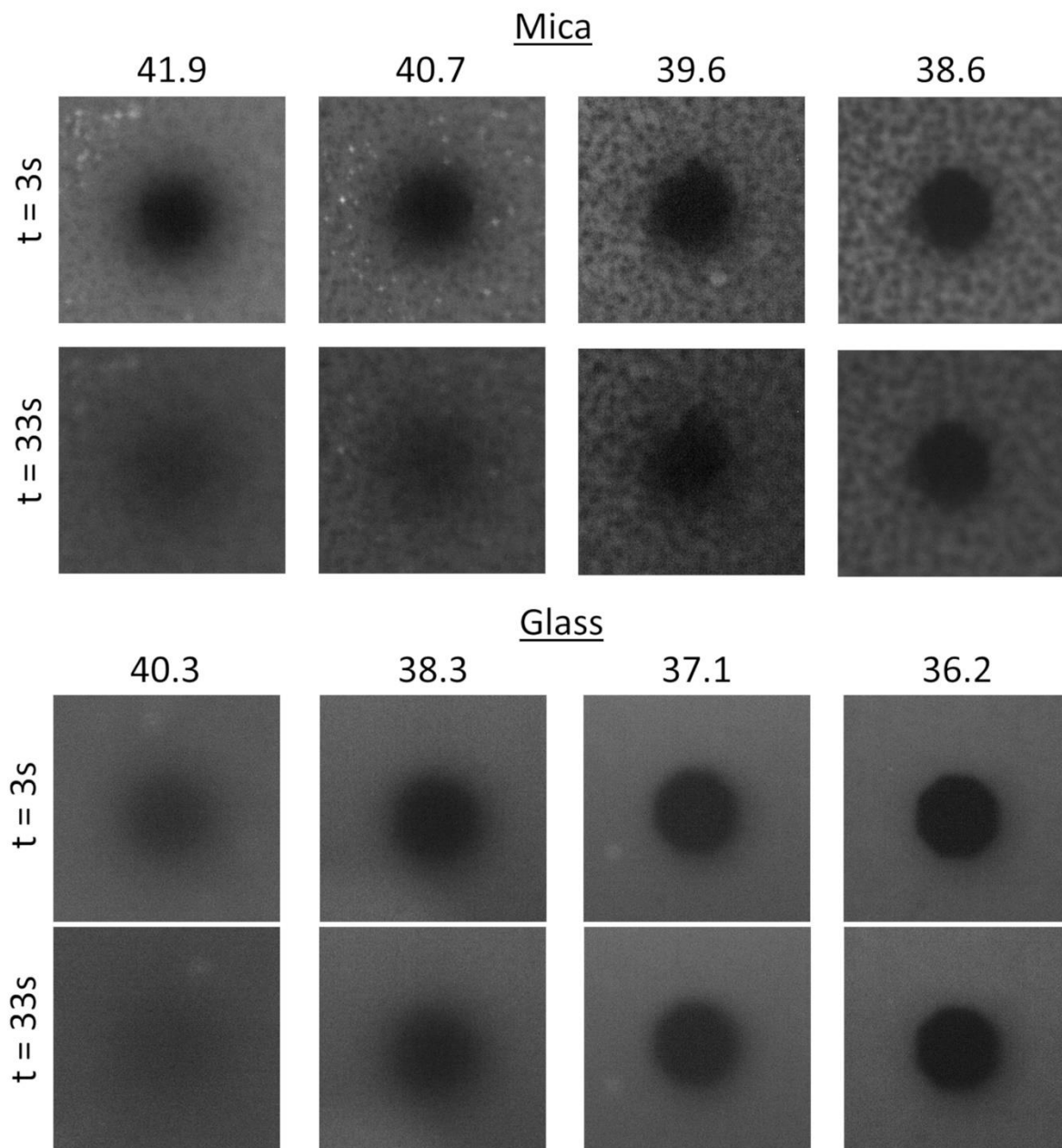


**Figure S8. FRAP on DPPC+ 0.5mol% NBD bilayer on glass as the bilayer cools. Fluorescence Images at 3s and 33s after photobleach at different temperatures, temperature is indicated above images.**